Cellular/Molecular

CLC Anion/Proton Exchangers Regulate Secretory Vesicle Filling and Granule Exocytosis in Chromaffin Cells

Maddalena Comini,[1*] Juan Sierra-Marquez,[1*] Gustavo Guzman,[2] Arne Franzen,[1] Antje Willuweit,[3] Istvan Katona,[4] Patricia Hidalgo,[1] Christoph Fahlke,[1] and Raul E. Guzman[1]

[1]Institute of Biological Information Processing, Molekular-und Zellphysiologie (IBI-1), Forschungszentrum Jülich, 52428 Jülich, Germany, [2]Institute of Neuroscience and Medicine (INM-10), Forschungszentrum Jülich, 52428 Jülich, Germany, [3]Institute of Neuroscience and Medicine (INM-4), Medical Imaging Physics, Forschungszentrum Jülich, 52428 Jülich, Germany, and [4]Institute of Neuropathology, RWTH Aachen University, 52056 Aachen, Germany

ClC-3, ClC-4, and ClC-5 are electrogenic chloride/proton exchangers that can be found in endosomal compartments of mammalian cells. Although the association with genetic diseases and the severe phenotype of knock-out animals illustrate their physiological importance, the cellular functions of these proteins have remained insufficiently understood. We here study the role of two *Clcn3* splice variants, ClC-3b and ClC-3c, in granular exocytosis and catecholamine accumulation of adrenal chromaffin cells using a combination of high-resolution capacitance measurements, amperometry, protein expression/gene knock out/down, rescue experiments, and confocal microscopy. We demonstrate that ClC-3c resides in immature as well as in mature secretory granules, where it regulates catecholamine accumulation and contributes to the establishment of the readily releasable pool of secretory vesicles. The lysosomal splice variant ClC-3b contributes to vesicle priming only with low efficiency and leaves the vesicular catecholamine content unaltered. The related Cl^-/H^+ antiporter ClC-5 undergoes age-dependent downregulation in wild-type conditions. Its upregulation in $Clcn3^{-/-}$ cells partially rescues the exocytotic mutant defect. Our study demonstrates how different CLC transporters with similar transport functions, but distinct localizations can contribute to vesicle functions in the regulated secretory pathway of granule secretion in chromaffin cells.

Key words: **anion/proton exchangers; chromaffin cells; ClC-3; exocytosis; neurosecretion**

Significance Statement

Cl^-/H^+ exchangers are expressed along the endosomal/lysosomal system of mammalian cells; however, their exact subcellular functions have remained insufficiently understood. We used chromaffin cells, a system extensively used to understand presynaptic mechanisms of synaptic transmission, to define the role of CLC exchangers in neurosecretion. Disruption of ClC-3 impairs catecholamine accumulation and secretory vesicle priming. There are multiple ClC-3 splice variants, and only expression of one, ClC-3c, in double Cl^-/H^+ exchanger-deficient cells fully rescues the WT phenotype. Another splice variant, ClC-3b, is present in lysosomes and is not necessary for catecholamine secretion. The distinct functions of ClC-3c and ClC-3b illustrate the impact of expressing multiple CLC transporters with similar transport functions and separate localizations in different endosomal compartments.

Introduction

Adrenal chromaffin cells are prototypic neuroendocrine cells and represent a well-established model for studying presynaptic nerve terminals at high temporal resolution. They release catecholamine into systemic circulation by exocytosis of large dense-core vesicles (LDCVs), which accumulate catecholamines via proton-coupled vesicular monoamine transporters (Yaffe et al., 2018). In chromaffin cells, LDCVs are organized in four different vesicle pools, the depot pool, the unprimed pool (UPP), the slowly releasable pool (SRP), and the readily releasable pool (RRP; Becherer and Rettig, 2006). Vesicles move from the depot pool to the membrane and form the UPP in a process known as docking. Subsequently, in the

Received Dec. 13, 2021; revised Feb. 2, 2022; accepted Feb. 7, 2022.

Author contributions: R.E.G., P.H., and C.F. designed research; R.E.G., M.C., J.S.-M., G.G., A.F., and I.K. performed research; A.W., R.E.G., M.C., J.S.-M., and G.G. analyzed data; R.E.G. and C.F. wrote the paper.

This work was supported by a grant from the Deutsche Forschungsgemeinschaft (GU 2042/2-1 to R.E.G). We thank Petra Thelen for technical assistance in molecular biology, Verena Graf for assistance in the quantitative PCR experiments, and Dr. Nicola Kornadt-Beck and the staff of our animal facility for support in all aspects of the animal work.

M. Comini's present address: Nuffield Department of Clinical Neurosciences, University of Oxford, Oxford OX3 9DU, United Kingdom

*M.C. and J.S.-M. contributed equally to this work.

The authors declare no competing financial interests.

Correspondence should be addressed to Raul E. Guzman at r.guzman@fz-juelich.de.

https://doi.org/10.1523/JNEUROSCI.2439-21.2022

Ca^{2+}-dependent step, the transition of vesicles from UPP to the slowly releasable pool (from which vesicles transit toward the RRP) is defined as priming (Becherer and Rettig, 2006). Physiologic stimuli cause an elevation of intracellular calcium concentrations and mainly trigger fusion of release-competent, or primed, vesicles from the RRP (Voets et al., 1999), making this vesicle pool the principal determinant of the high spatiotemporal accuracy of catecholamine secretion (Schoch et al., 2001; Sørensen et al., 2003; Dhara et al., 2014; Mishima et al., 2014).

CLC chloride transporters have been proposed to contribute to vesicular acidification, neurotransmitter filling, and trafficking of intracellular organelles in various cells (Stauber and Jentsch, 2010, 2013). Adrenal chromaffin cells express all CLC antiporters (Maritzen et al., 2008), but their functions and subcellular localizations have remained largely controversial (Barg et al., 2001; Maritzen et al., 2008; Deriy et al., 2009; Li et al., 2009; Jentsch et al., 2010). In experiments using ClC-3 antibodies with KO staining-controlled specificity, Maritzen et al. (2008) did not find ClC-3 in secretory granules of adrenal chromaffin cells and pancreatic islet cells. The authors observed reduced exocytotic responses and lower catecholamine content in *Clcn3*$^{-/-}$ chromaffin cells and postulated an indirect role of this transporter in exocytosis. Other groups reported localization in secretory vesicles and direct regulation of intragranular pH and secretion of insulin-containing granules by ClC-3 in pancreatic β-cells (Barg et al., 2001; Deriy et al., 2009); however, antibodies were not tested for specificity in *Clcn3*$^{-/-}$ animals.

There are multiple splice variants of *Clcn3*, and, thus far, the contributions of these distinct ClC-3 splice variants to chromaffin function have not been addressed. We combined high-resolution membrane capacitance measurements, amperometric recordings, and confocal images to identify cellular roles of ClC-3 splice variants. We aimed to determine the subcellular localization of ClC-3b and ClC-3c and elucidated at which vesicular maturation step Cl^-/H^+ exchanger regulates exocytosis in chromaffin granules. We found that the exocytosis of secretory granules and their catecholamine content are reduced in the absence of ClC-3. Rescue experiments from double Cl^-/H^+ exchanger-deficient cells revealed that expression of ClC-3c fully restore transmitter content and granule exocytosis. Expression of ClC-3b did not alter catecholamine accumulation of single secretory granules but partially rescued exocytosis in cells lacking ClC-3 and ClC-5. Our results demonstrate that ClC-3c is present in a subpopulation of large dense-core vesicles and directly regulates catecholamine accumulation and exocytosis in chromaffin cells, whereas ClC-3b contributes to the priming of secretory granules but is not involved in the process of neurotransmitter accumulation.

Materials and Methods

Mutant mice and cell culture. *Clcn3*$^{-/-}$ mice, provided by Thomas Jentsch (Leibniz-Forschungsinstitut für Molekulare Pharmakologie; Stobrawa et al., 2001), were maintained as heterozygotes by continuous cross-breeding with C57BL/6. Knock-out and WT littermates of either sex were obtained by crossing heterozygotes and were identified by PCR genotyping. Preparation and cultivation of adrenal chromaffin cells were performed as described previously (Sørensen et al., 2003; Borisovska et al., 2005). In brief, adrenal glands were removed and enzymatically treated (12 U/ml papain; Worthington Biochemical) for 20 min. Subsequently, cells were seeded on glass coverslips after trituration and cultured at 37°C and 10% CO_2 in enriched DMEM [100 ml DMEM supplemented with 0.4 ml penicillin/streptomycin, 1 ml sodium pyruvate (100 mM), and 1 ml insulin-transferrin-selenium-X; Invitrogen]. For lentiviral transduction, the viral suspension was added 2 h after plating. Patch-clamp and amperometric recordings were performed at room temperature either on the second or third day *in vitro* or 4–5 d after infection of the cells with viral particles. For confocal microscopy, cells were seeded on poly-D-lysine (catalog #P6407, Sigma-Aldrich) coated coverslips.

Electrophysiology. Whole-cell voltage-clamp recordings were performed using an EPC10 amplifier controlled by PatchMaster (HEKA Elektronik). Photolysis of caged Ca^{2+} and ratiometric measurements of intracellular calcium concentration were conducted as previously described (Borisovska et al., 2005). The standard extracellular solution consisted of the following (in mM): 130 NaCl, 4 KCl, 2 $CaCl_2$, 1 $MgCl_2$, 10 HEPES, 48 D-glucose, pH 7.4, with NaOH. For flash photolysis experiments, pipettes with resistances between 3 and 4 MΩ were filled with the following (in mM): 110 Cs-Glutamate, 8 NaCl, 3.5 CaCl2, 5 NP-EGTA (provided by Dieter Bruns, University of Homburg, Germany), 0.2 Fura-2, 0.3 Furaptra (Thermo Fisher Scientific), 2 MgATP, 0.3 Na_2GTP, 40 HEPES, pH 7.3, 320 mOsm. NP-EGTA was photolyzed by a flash of ultraviolet light (Xenon flash lamp, Rapp OptoElectronics) focused through an Olympus objective (60×, UPlanSApo, 1.35 oil) of an inverted microscope (IX71, Olympus). Fura-2 and Furaptra were excited at 350/380 nm using a monochromator light. To maintain high $[Ca^{2+}]_{int}$, after the flash small amounts of NP-EGTA were photolyzed. For quantifying depolarization-induced secretion we used patch pipettes with resistances between 3 and 4 MΩ and containing the following (in mM): 120 Cs-glutamate, 8 NaCl, 0.18 $CaCl_2$, 0.28 BAPTA, 1 $MgCl_2$, 2 MgATP, 0.5 Na_2GTP, 10 HEPES-CsOH, pH 7.3, 350 nM calculated free $[Ca^{2+}]_{int}$, 290 mOsm, pH 7.4. Capacitances were measured using the Lindau-Neher technique (sine wave stimulus, 1000 Hz, 35 mV peak-to-peak amplitude, DC-holding potential −70 mV) using the lock-in extension of Patchmaster (HEKA Elektronik). Currents were low-pass filtered at 2.9 kHz and digitalized with a sampling rate of 20 kHz. Membrane capacitance was analyzed using SigmaPlot 12.3 software with customized routines (Systat Software). The flash-evoked capacitance response was fit with $f(t) = A_0 + A_1(1\text{-}\exp^{-t/\tau 1}) + A_2(1\text{-}\exp^{-t/\tau 2}) + kt$. A_0 denotes the cell capacitance before the flash, and A_1, τ_1 and A_2, τ_2 represent amplitudes and time constants of RRP and SRP, respectively (Rettig and Neher, 2002). Ca^{2+} currents from cultured chromaffin cells were measured as described by Toft-Bertelsen et al. (2016). The standard extracellular solution contained the following (in mM): 135 NaCl, 10 HEPES, 2.8 KCl, 10 $CaCl_2$, 1 $MgCl_2$, 11 D-glucose, and 1 μM tetrodotoxin. The patch-pipette solution contained the following (in mM): 112.5 CsGlut, 36 HEPES, 9 NaCl, 3 MgATP, 0.45 Na_2GTP, and 10 EGTA (300 mOsm, pH 7.2). Ca^{2+} currents were measured during 100 ms test pulses ranging from −70 to +120 mV in 10 mV increments from a holding potential of −70 mV. We determined the voltage dependence of channel activation by plotting tail current amplitudes measured at fixed-test step to −50 mV following the variable test pulses applied.

Carbon fiber electrodes (7 μm diameter, Goodfellow) were prepared as previously described (Guzmán et al., 2007). Amperometric recordings were performed under voltage-clamp conditions with a polarization potential of +800 mV, filtered at 2.9 kHz, and sampled at 20 kHz, and analyzed using Origin (OriginLab) and an Igor-based macro (IgorPro 7.01, WaveMetrics) developed in Sulzer Lab (https://github.com/DSulzerLab/Quanta_analysis). The analysis was restricted to events with peak amplitude >7 pA, total charge >10 fC, and 50–90% rise time faster than 0.9 ms. Foot signal events >2 ms in duration were analyzed. For K^+-induced secretion, the external solution [containing the following (in mM): 50 NaCl, 80 KCl, 2 $CaCl_2$, 1 MgCl, 48 glucose, 10 HEPES, pH 7.3, adjusted with NaOH] was applied from a perfusion pipette. Only one recording was made per coverslip to avoid the fatigue of the secretory response. For calcium infusion experiments, the pipettes solution contained the following (in mM): 110 Cs-glutamate, 8 NaCl, 1 $CaCl_2$, 20 DPTA, 1 $MgCl_2$, 2 MgATP, 0.5 Na_2GTP, 40 HEPES-CsOH, pH 7.3, 3 μM calculated free $[Ca^{2+}]_{int}$.

Expression constructs and lentiviral production. We constructed the RNA-polymerase III promoter based on the lentiviral backbone vector

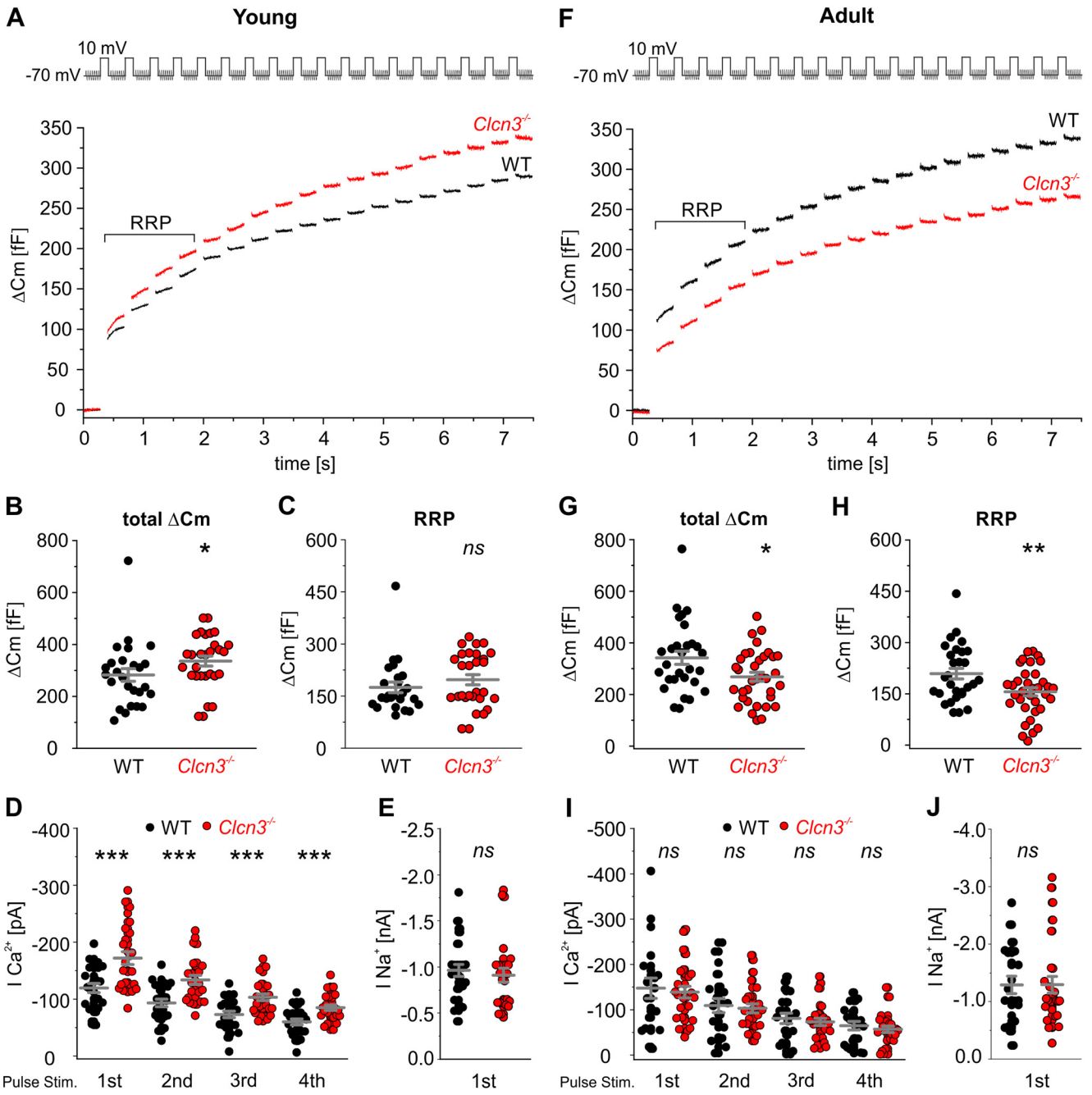

Figure 1. Exocytosis triggered by trains of depolarizing steps is impaired in *Clcn3*$^{-/-}$ cells from adult mice. ***A***, Schematic representation of the depolarization protocol used to trigger exocytosis of secretory vesicles (top, 18 pulses, 100 ms to +10 mV delivered with 300 ms rest intervals) and the averaged ΔCm responses from WT and for *Clcn3*$^{-/-}$ cells obtained from P0 (postnatal day zero) mice (bottom). ***B***, Mean value for the total ΔCm in newborn WT or *Clcn3*$^{-/-}$ chromaffin cells. ***C***, Mean sizes of the RRP from newborn WT or *Clcn3*$^{-/-}$ chromaffin cells. ***D***, ***E***, The amplitude of the Ca^{2+} currents measured during the first four depolarization episodes but not the Na^{+} currents measured at the first depolarization step, was significantly higher in the *Clcn3*$^{-/-}$ chromaffin cells from young mice. ***F***, Schematic representation of the depolarization protocol used to trigger secretion (top, 18 pulses, 100 ms to +10 mV delivered with 300 ms rest intervals) and the averaged ΔCm responses in adult WT or *Clcn3*$^{-/-}$ cells (bottom). ***G***, Mean value for the total ΔCm from adult WT or *Clcn3*$^{-/-}$ cells. ***H***, Mean sizes of the RRP from adult WT or *Clcn3*$^{-/-}$ cells. ***I***, ***J***, The amplitude of the Ca^{2+} currents measured during the first four depolarization episodes and Na^{+} currents measured at the first depolarization step were similar between WT and *Clcn3*$^{-/-}$ chromaffin cells isolated for adult mice. Young mice: WT, $n = 25$, black circles; *Clcn3*$^{-/-}$, $n = 26$, red circles; adult mice: WT, $n = 29$, black circles; *Clcn3*$^{-/-}$, $n = 35$, red circles, ***$p < 0.001$, **$p < 0.01$, *$p < 0.05$. ns, Not significant. n, denotes the number of analyzed cells. Student's *t* test. Data were collected from five independent experiments per condition and are represented as mean ± SEM.

FsY 1.1-eGFP G.W. (provided by Mikhail Filippov, Nizhny Novgorod, Russia). The human H1 promoter was cloned upstream of the synapsin promoter (H1-FsY1.1-eGFP), and the short-hairpin targeting sequence found in the mouse ClC-5 nucleotide sequence NM_016691.2 (CCTATGATGATTTCAACACAA) was cloned downstream of the H1 promoter (H1-shRNA-FsY 1.1-eGFP, Sigma-Aldrich; Clone ID, NM_016691.2-240s1c1; TRC number, TRCN0000069494, mean knock-down level of 94% and mean knockdown level tested in chromaffin cell cultures was of 92.6%, $n = 8$ cultures). In addition, a scrambled shRNA sequence (ACTACCGTTGTTATAGGTG) was inserted into the same vector and used as a control for all shRNA experiments (H1-shRNA*scr*-FsY 1.1-eGFP). To rescue ClC-3 function, the ClC-3 promoter was cloned downstream of the H1-shRNA sequence, replacing the synapsin promoter (H1-shRNA-FpromClC-3 1.1-eGFP). We cloned the *Mus musculus* ClC-3b and ClC-3c sequence downstream to the

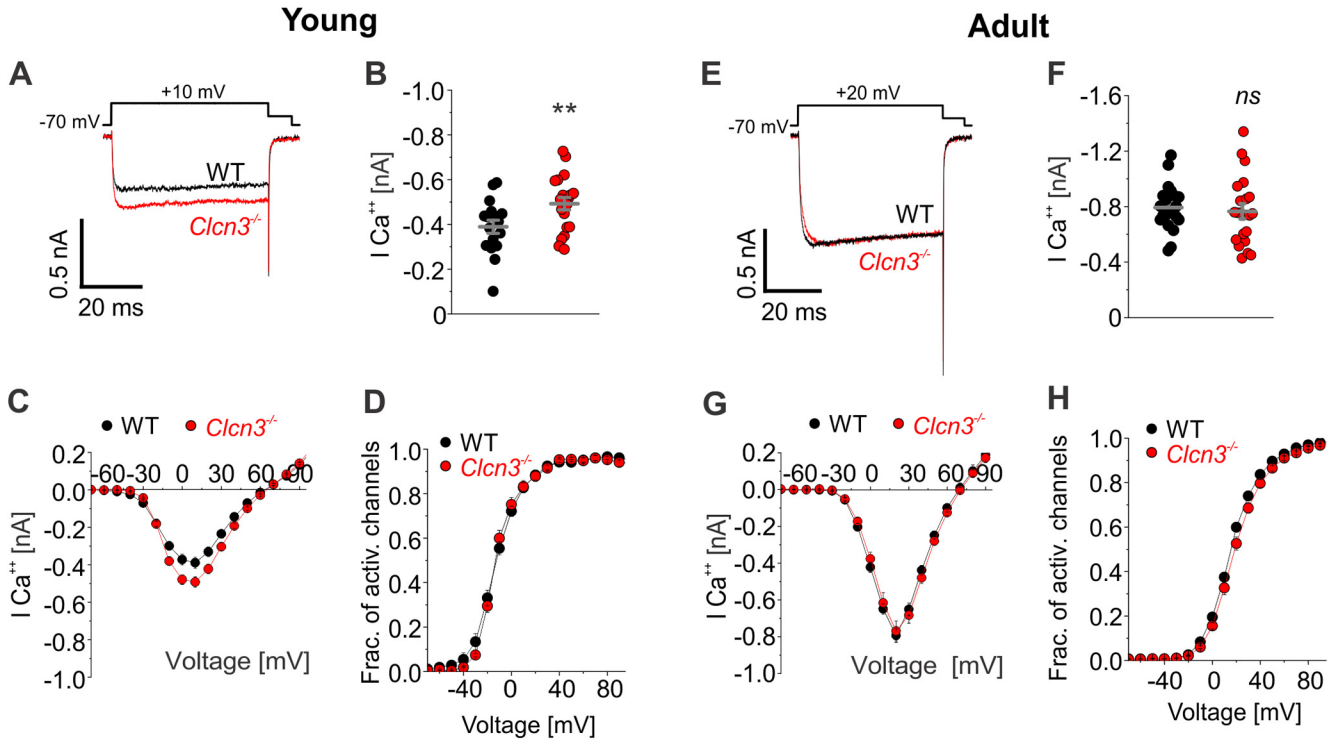

Figure 2. Calcium currents are increased in $Clcn3^{-/-}$ cells from young mice. ***A***, Voltage protocol to activate VGCC (top) and representative calcium currents of WT (black) and $Clcn3^{-/-}$ (red) cells from young animals. ***B***, Deletion of ClC-3 increases calcium current amplitudes when compared with WT chromaffin cells, (WT, $n = 25$, black circles, and $Clcn3^{-/-}$, $n = 29$, red circles). ***C***, Voltage dependence of steady-state current amplitudes for WT (black) or $Clcn3^{-/-}$ (red) chromaffin cells. ***D***, Deletion of ClC-3 does not affect the voltage dependence of calcium current activation, WT ($n = 17$, black) and $Clcn3^{-/-}$ ($n = 20$, red). ***E***, Voltage protocol to activate VGCC (top) and representative calcium currents of WT (black) and $Clcn3^{-/-}$ (red) cells from adult animals. ***F***, In contrast to young, $Clcn3^{-/-}$ adult chromaffin cells do not show changes in the peak of calcium current amplitude when compared with the control, (WT, $n = 20$, black circles, and $Clcn3^{-/-}$, $n = 21$, red circles). ***G***, Voltage dependence of steady-state current amplitudes for WT (black) or $Clcn3^{-/-}$ (red) chromaffin cells from adult mice. Note that the peak of the calcium current amplitude measured in chromaffin cells from adult mice has shifted 10 mv to the right (+20 mv) when compared with those measured from young cells. ***H***, Deletion of ClC-3 does not affect the voltage dependence of calcium current activation, WT ($n = 20$, black) and $Clcn3^{-/-}$ ($n = 21$, in red), $^{**}p < 0.01$. ns, Not significant. Student's *t* test. Data were collected from four independent experiments per condition and are represented as mean ± SEM; *n* denotes the number of analyzed cells.

ClC-3 promoter, followed by 2A self-cleaving sequence and eGFP (FpromClC-3c 1.1-eGFP or H1-shRNA- FpromClC-3c 1.1-eGFP). The genomic localization of the promoter sequence used in this study is chromosome 8, NC_000074.6 (from 60955251–60954643). This position is located right in front of the starting codon of ClC-3c and is different from the promoter sequence of the other ClC-3 splice variants. ClC-3c (GenBank accession no. NM_173876.3) or ClC-3b (GenBank accession no. NM_173873.1; O'Leary et al., 2016). An empty vector carrying ClC-3c promoter and eGFP was used as a control (FpromClC-3c 1.1-eGFP). Lentiviral particles were produced as described previously (Guzman et al., 2010) by coexpressing lentiviral expression vectors, the helper plasmids pRSVREV and pMDLg/pRRE, and vesicular stomatitis virus G-protein-expressing plasmid (provided by Thomas Südhof, Howard Hughes Medical Institute, Stanford University) in HEK293FT cells. The culture medium containing lentiviral particles was collected 72 h post-transfection and ultracentrifuged for 2 h. Lentiviral particles were immediately resuspended in culture medium, frozen in liquid nitrogen, and stored at −80°C.

Confocal microscopy. Lentiviral transduction was used to express ClC-3b and ClC-3c (Guzman et al., 2015) in combination with fluorescent markers such as Lamp1 (which was a gift from Walther Mothes, plasmid #1817, Addgene; http://www.addgene.org/1817; RRID:Addgene_1817; Sherer et al., 2003); Rab7, Rab11 (a gift from Richard Pagano, plasmid #12605 and #12674, Addgene; Choudhury et al., 2002); TfR (a gift from Gary Banker, plasmid #45060 Addgene; Burack et al., 2000); and VAMP3 and VAMP4 (a gift from Thierry Galli, plasmid #42310 and #42313, Addgene; Galli et al., 1998). Chromogranin A and neuropeptide Y were cloned into the p156rrL lentivector (Guzman et al., 2010) using genomic cDNA isolated from mouse adrenal gland and using the following set of primers: Chromogranin A (GenBank accession no. NM_007693.2; O'Leary et al., 2016), forward 5′- ATGCGCTCCACCGCGGTTCTG-3′, reverse 5′-TCCCCGCCGCAAAGCCTGC-3′, and neuropeptide Y (GenBank accession no. NM_023456.3; O'Leary et al., 2016), forward 5′-ATGCTAGGTAACAAGCGAATGGGGC-3′ and reverse 5′-CCACAT GGAAGGGTCTTCAAGCC-3′. Chromaffin cells were imaged 4–5 d after transduction with a Leica TCS SP5 II inverted microscope (Leica Microsystems) using a 63× oil immersion objective in PBS containing Ca^{2+} and Mg^{2+} (Invitrogen) at room temperature (22–24°C). eGPF (enhanced green fluorescence protein) fluorophore was excited with a 488 nM Argon laser, mRFP (monomeric red fluorescence protein) with a 594 nM He-Ne laser, and emission signals were detected after filtering at 500–550 nm or 600–650 nm bandpass filters. WT or $Clcn3^{-/-}$ chromaffin cells from postnatal day (P)0–P1 were used for immunostaining after 4 d of culture. Cells were fixed for 10 min with 4% paraformaldehyde and permeabilized for 1 h with a solution containing the following: 0.5% Triton 100, 5% fetal bovine serum, and 0.5% bovine serum albumin in phosphate buffer, pH 7.4. Thereafter the samples were immunostained using the primary ClC-3 antibodies, rabbit anti-ClC-3 ACL-001 (Alomone Labs) or

Table 1. mRNA Transcripts levels of ClC-3 and ClC-5 in mouse adrenal gland

	Log [cDNA] 18S in WT	Log [cDNA] ClC-3 in WT	Log [cDNA] ClC-5 in WT	Log [cDNA] ClC-5 in $Clcn3^{-/-}$
P0	6.80 ± 0.20	3.90 ± 0.05	2.70 ± 0.20	3.1 ± 0.15*
P60	6.70 ± 0.40	3.80 ± 0.08	1.80 ± 0.20*	

Adrenal glands were collected from C57BL/6 mouse strain at two different developmental stages, P0 (postnatal day 0) ($n = 5$) and P60 (postnatal day 60) ($n = 3$) or $Clcn3^{-/-}$ mice at P0 ($n = 5$). $^{*}p < 0.05$; Student©s *t* test. cDNA samples were measured in triplicate and are represented as mean ± SEM n, denotes the number of analyzed cells.

rabbit anti-ClC-3 C9602 (Sigma-Aldrich), at the concentration suggested by the manufacturer or using 1:100 dilution (both concentrations gave similar results) and mouse anti-chromogranin A (catalog #Ab8204, Abcam) or with mouse anti-LAMP1 (catalog #H4A3 Sc-20 011, Santa Cruz Biotechnology) using the concentrations recommended by the manufacturer. Samples were washed twice and incubated with the secondary antibody (rabbit Alexa Fluor 488 and mouse Alexa Fluor 647, 1:1000, in phosphate buffer, catalog #A-11008 and #A-31571, Invitrogen). To determine the degree of colocalization between ClC-3b or ClC-3c or the anti-ClC-3 ACL-001 antibody and the different intracellular markers, the subcellular localization was quantified in confocal images as mRFP fluorescence intensity overlapping with eGFP fluorescence or Alexa 488 fluorescence intensity overlapping with Alexa 647 signal using Mander's overlap coefficient. Images were analyzed and assembled for publication in ImageJ 1.44p software (National Institutes of Health; Schneider et al., 2012).

Electron microscopy. Adrenal glands from WT and *Clcn3*$^{-/-}$ littermates (P0–P1) were fixed for 24 h with 2.5% glutaraldehyde in 0.1 M phosphate buffer at room temperature. After fixation, glands were washed with phosphate buffer for a further 24 h, treated with 1% OsO4 (in 0.2 M phosphate buffer) for 3 h, washed twice with distilled water, and dehydrated using ascending alcohol concentrations (25–100%). Dehydrated glands were incubated with propylene oxide followed by an additional 20 min incubation with a 1:1 mixture of Epon containing propylene oxide [Epon; 47.5% glycidether, 26.5% dodenylsuccinic acid anhydride, 24.5% methylnadic anhydride, and 1.5% Tris (dimethylaminomethyl)phenol)]. Thereafter, samples were immersed in pure epoxy resin for 1 h at room temperature followed by polymerization (28°C for 8 h, 80°C for 2.5 h, and finally at room temperature for 4 h). Ultrathin sections (~60–80 nm thickness) were mounted on copper grids. To enhance contrast, sections were treated with uranyl acetate and lead citrate. Samples were examined using an EM900 electron microscope (Zeiss) equipped with a slow-scan CCD Camera (TRS). We only used sections containing cells with visible nucleus and identified secretory vesicles by their round electron-dense core. For each condition, different fields of view were analyzed, the number of vesicles was counted in this area, and the diameter of secretory vesicles was measured. Data are presented as mean ± SEM, with *n* indicating the number of vesicle. Statistical comparisons were made using one-way ANOVA (Tukey's test).

RNA isolation and qRT-PCR. Adrenal glands were collected from C57BL/6 mouse strain at two different developmental stages, P0 ($n = 5$ mice) and P60 ($n = 3$) or *Clcn3*$^{-/-}$ mice at P0 ($n = 5$). RNA was isolated using the TRIzol Reagent method following instructions from the manufacturer (catalog #15596026, Thermo Fisher Scientific). In brief, 20 mg of tissue sample were homogenized in 1 ml of TRIzol, mixed with chloroform, and vigorously shaken for 15 s. After 2–3 min incubation at room temperature, the sample was centrifugated at 12.000 × *g* for 20 min at 4°C. The upper aqueous phase containing the RNA was separated, mixed with isopropanol by vortexing, and incubated for 10 min at room temperature. After centrifugation at 12.000 × *g* for 10 min at 4°C, the supernatant was discarded, and the pellet was washed with 75% ethanol, vortexed, and centrifuged at 7.500 × *g* for 5 min at 4°C. The pellet was dried for 15–20 min and resuspended in 20 µl of RNAase-free water. Genomic DNA was eliminated by treating the isolated RNA with DNAase using the DNAase I kit (catalog #18068015, Thermo Fisher Scientific). To evaluate the expression of the different CLC exchangers, we performed RT-PCR using 1 µg of total RNA, SuperScript III One-step RT-PCR system (catalog #12574, Invitrogen), and the following set of primers; ClC-3a (GenBank accession no. NM_007711.3; O'Leary et al., 2016); 5′-CGCCCAGCTTGCTATGCCTCTGAG-3′, reverse 5′-AGCTAGTGCCCCTGATGCCAGTC-3′; ClC-3b (GenBank accession no. NM_173873.1; O'Leary et al., 2016) 5′-CGCCCAGCTTGCTATGCCTCTGAG-3′, reverse 5′-AGCTAGTGCCCCTGATGCCAGTC-3′; ClC-3c (GenBank accession no. NM_173876.3; O'Leary et al., 2016) 5′-ATGGATGCTTCTTCTGATCC-3′, reverse 5′-AGCTAGTGCCCCTGATGCCAGTC-3′; ClC-3e (GenBank accession no. NM_173874.1; O'Leary et al., 2016) 5′-TGCCCTCAGAAGAGACCTGACTATTGC-3′, reverse 5′-AACGAACTTCCTCTTCTGTCTCCTCTCTG-3′; ClC-5 isoform 2 (GenBank accession no. NM_001243762.1; O'Leary et al., 2016) 5′-CAGAGGCTTTCATCAGGGGAGTTTTAG-3′, reverse 5′-CTCAGAATTCCAGCAACAGTGCTCATG-3′; and the reference gene 18S rRNA 5′- CGCCGCTAGAGGTGAAATTCTTG-3′, reverse 5′-GTGGCTGAACGCCACTTGTCC-3′ was used. For quantitative (q)RT-PCR, cDNA from the total RNA was synthesized by mixing 1 µg of total RNA with 2.5 µM oligo(dT)18 (catalog #SO132, Thermo Fisher Scientific) and heating the mixture for 5 min at 65°C. After brief centrifugation, RNaseOUT recombinant RNase inhibitor (40 units/µl, catalog #10777-019, Thermo Fisher Scientific) and SuperScript III RT (200 units/µl) were added. The samples were incubated at 50°C for 1 h, subsequently inactivated at 70°C for 15 min, and the newly synthesized cDNA was used for qRT-PCR. Control reactions using no reverse transcriptase or substituting cDNA with water were run in parallel for each sample. Two sets of gene-specific primers were designed for ClC-3 and ClC-5 to recognize sequences in the coding region of the mouse *Clcn3* (GenBank accession no. NM_007711.3) and *Clcn5* (GenBank accession no. NM_001243762.1) that allow amplification of all existing splice variants; for ClC-3, forward 5′-CCTCTTATGGCTGCAGTAATGACC-3′, reverse 5′-GCACTGCCTCAGACCAAGCTT-3′; ClC-5, forward 5′-CAGAGGCTTTCATCAGGGGAGTTTTAG-3′ reverse 5′-CTCAGAATTCCAGCAACAGTGCTCATG-3′; and for the reference genes 18S (GenBank accession no. NR_003278.3), forward 5′-CGCCGCTAGAGGTGAAATTCTTG-3′, reverse 5′- GTGGCTGAACGCCACTTGTCC-3′ and GFP forward 5′- TTCATCTGCACCACCGGCAA-3′, reverse 5′- TTGGGGTCTTTGCTCAGGGC-3′. The qRT-PCR was performed on 96 well plates using the Maxima SYBER Green qPCR Master Mix (catalog #K0251, Thermo Fisher Scientific) and run on a Bio-Rad Laboratories instrument (thermal cycle C1000 Touch, CFX96 real-time system). The transcription levels of ClC-3 and ClC-5 were analyzed and compared with that of the reference gene (18S). Three separate analyses of PCR were performed. The data were analyzed according to the CFX manager (Bio-Rad) recommended protocols.

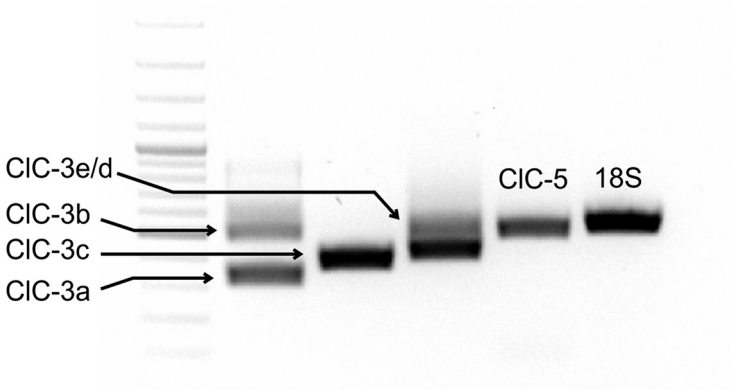

Figure 3. Expression of ClC-3 and ClC-5 in mouse adrenal gland. The expression of Cl^-/H^+ exchangers in adrenal glands was examined by RT-PCR. The expected PCR product size obtained for each transporter revealed the presence of mRNA transcripts of ClC-3 splice variants and ClC-5 in this tissue. Mouse adrenal glands were collected from five P0-P1 (postnatal days 0-1) mice and pooled together.

Statistical analysis. Statistical calculations were performed using SigmaPlot software, version 12.3; Systat Software; and Origin(Pro), version 2018 (OriginLab). All summary data are given as mean ± SEM. The comparison was made using a *t* test of means or ANOVA after passing assumptions of normality (Shapiro–Wilk test) and equal variances (Levene's test) or Mann–Whitney rank sum test with $*p < 0.05$, $**p < 0.01$, and $***p < 0.001$ levels of significance. Grubbs' test was performed to test for outliers.

Animal maintenance . The animals were maintained according to the guidelines of the Federation of European laboratory Animal Science Association, and the breeding for the ClC-3^{KOTje} mouse line was approved by the Landesamt für Natur, Umwelt und Verbraucherschutz Nordrhein-Westfalen, Aktenzeichen No. 84–02.04.2015.A108.

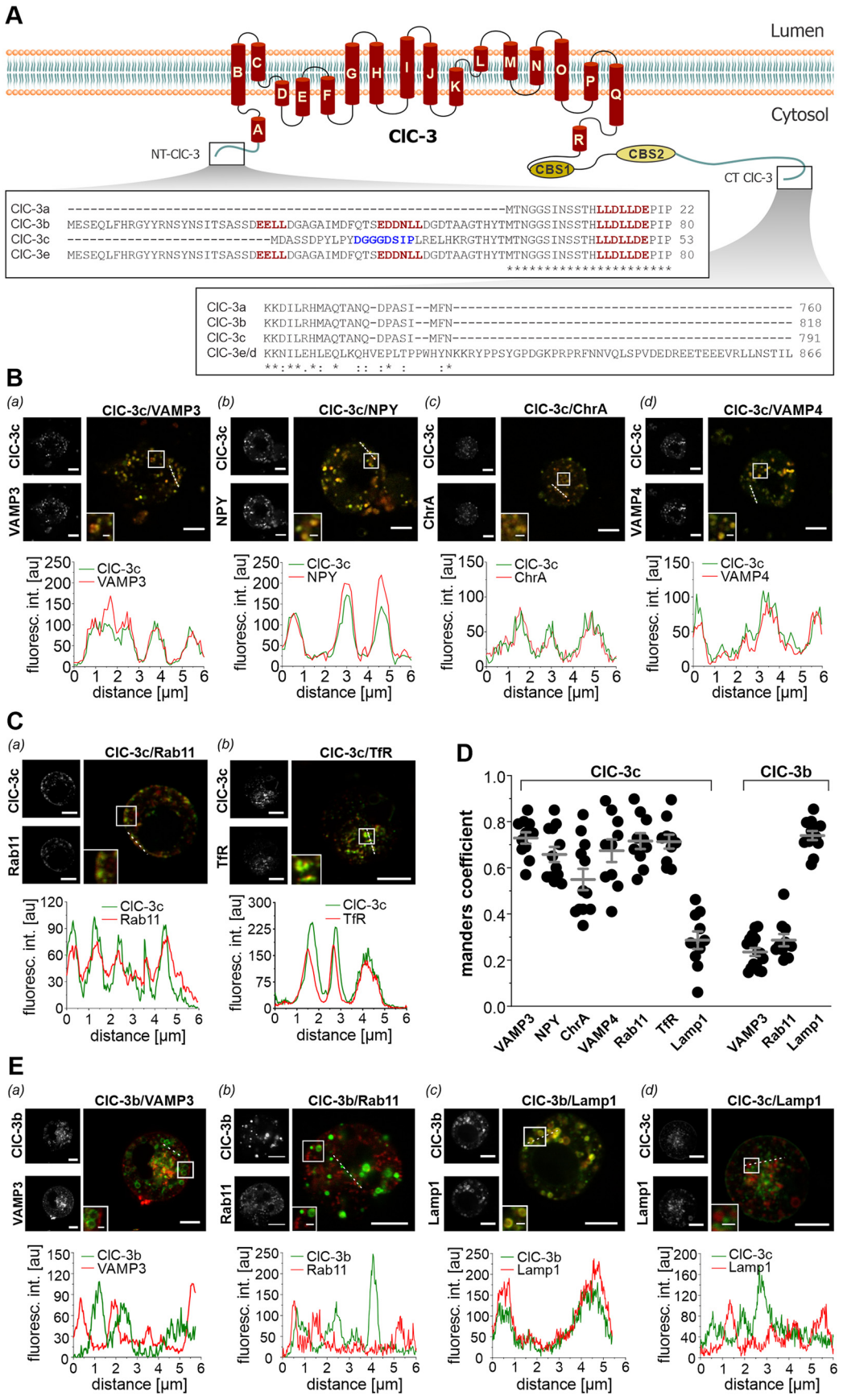

Figure 4. Subcellular localization of ClC-3 splice variants. ***A***, Diagram of the protein topology model of ClC-3 illustrating the transmembrane and cytoplasmic domains. The 18 α helices are labeled A–R, the two cytoplasmic cystathionine β-synthase (CBS) domains are shown in ovals (CBS1 and CBS2). The amino acid sequence of the cytoplasmic N- and C-amino termini are shown within the rectangles. Highlighted in red, we illustrated the clathrin binding dileucine motif and in blue, the recycling endosomes targeting signal. Note that ClC-3b and ClC-3c differ

Results

ClC-3 regulates granule exocytosis in chromaffin cells

We studied granule exocytosis in chromaffin cells from newborn and adult mice on trains of depolarizing pulses using time-resolved capacitance measurements. Such pulses increase $[Ca^{2+}]_i$ at the plasma membrane via activation of voltage-gated calcium channels and trigger the fusion of vesicles that are in close proximity to the calcium channels. We used a series of depolarizations (18 pulses, 100 ms to +10 mV delivered with 300 ms resting intervals at −70 mv) that is known to effectively deplete the RRP within the first four pulses of the stimulus trains but to be ineffective in releasing vesicles from the SRP (Voets et al., 1999). In chromaffin cells prepared from newborn mice, the total capacitance changes elicited by this stimulation protocol were larger in *Clcn3*$^{-/-}$ chromaffin cells than in WT. However, the fourth step of depolarization, which defines the size of the RRP, was not different between WT and *Clcn3*$^{-/-}$ (Fig. 1*A–C*). The amplitude of the Ca^{2+} current component during the first four depolarization episodes was on average 1.4 ± 0.08-fold higher in chromaffin cells isolated from young *Clcn3*$^{-/-}$ mice than for WT (Fig. 1*D*). Na^+ currents were not altered in young *Clcn3*$^{-/-}$ cells (Fig. 1*E*). In cells from adult mice, we found the first four capacitance responses within the stimulus train to be reduced in *Clcn3*$^{-/-}$ (Fig. 1*F–H*), with unchanged calcium and sodium current amplitudes (Fig. 1*I,J*). Because exocytosis is triggered by Ca^{2+} influx in these experiments, the age-dependent differences might be because of regulatory adjustments in the number or function of voltage-gated Ca^{2+} channels. We therefore isolated Ca^{2+} currents with Cs^+-based intracellular solution and 2 μM of tetrodotoxin in the bath solution to block K^+ and Na^+ currents; these experiments revealed a 1.5 ± 0.25-fold increase in peak calcium current amplitudes in juvenile *Clcn3*$^{-/-}$ cells, with no changes in the voltage dependence of channel activation (Fig. 2*A–D*). Adult *Clcn3*$^{-/-}$ cells did not show differences in the peak calcium current amplitudes when compared with the WT.

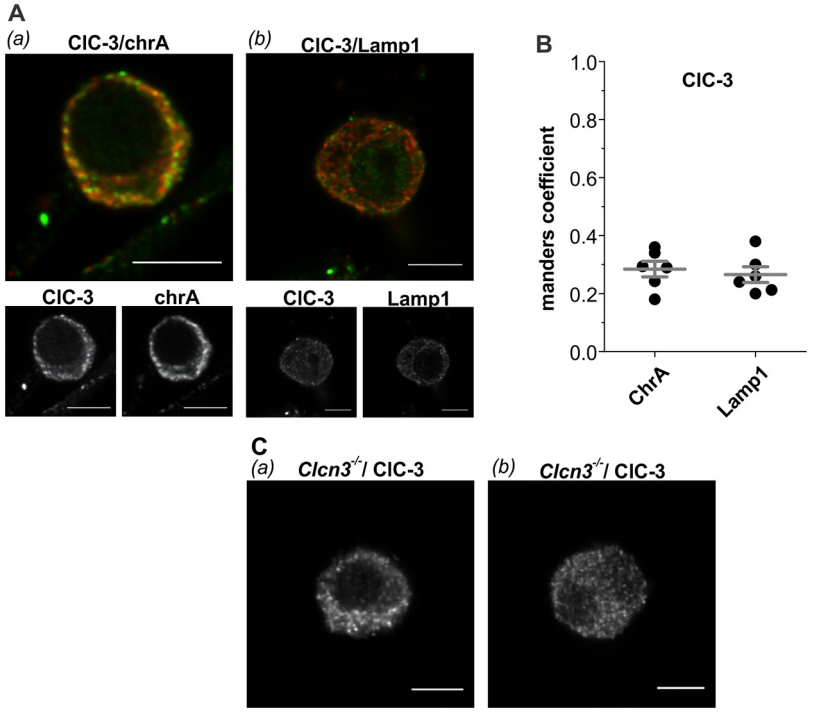

Figure 5. Commercially available ClC-3 antibodies are unspecific and failed in identifying ClC-3 in chromaffin cells. ***A***, Confocal images of WT chromaffin cells from P0-P1 (postnatal days 0-1) mice immunostained with ClC-3 antibody (ACL-001) together with chromogranin A *(a)*, a marker for large dense-core vesicles or with LAMP1 *(b)*, a lysosomal marker. ***B***, Mander's coefficient analyses indicate not colocalization with chromogranin A ($n = 6$) or with LAMP1 ($n = 6$). ***C***, Confocal pictures of *Clcn3*$^{-/-}$ chromaffin cells from P0-P1 (postnatal days 0-1) mice immunostained with ClC-3 antibody (ACL-001) *(a)* or with ClC-3 antibody (C9602). Note that both antibodies stained intracellular structures in the absence of ClC-3. All data are represented as mean ± SEM; *n* denotes the numbers of cells analyzed. Scale bars: 5 μm; insets, 1 μm. The immunostainings were performed from preparations from two different animals.

Constitutive genetic ablation often causes compensatory changes in expression levels of other proteins. Therefore, we hypothesized that other proteins with similar functions as ClC-3, for example, ClC-4 or ClC-5, might compensate exocytosis in the *Clcn3*$^{-/-}$ condition at an early developmental stage and increase the number of voltage-gated calcium channels at the plasma membrane. ClC-4 and ClC-5 are also present in adrenal glands (Maritzen et al., 2008) and exhibit functional properties comparable to those of ClC-3 (Guzman et al., 2013). Because ClC-4 lacks an endosomal trafficking signal and requires association with ClC-3 to be exported from the endoplasmic reticulum to endosomal compartments (Guzman et al., 2017), it is unlikely that ClC-4 exerts direct effects on exocytosis in *Clcn3*$^{-/-}$ condition. Therefore, we focused on ClC-5 and quantified mRNA transcripts levels in WT mice at two different ages, P0 and P60. We found ClC-5 transcripts to be reduced by ~70% in adult mouse adrenal tissue as compared with WT newborn condition (Log [cDNA] = 2.7 ± 0.2 for ClC-5 in WT P0 vs for ClC-5 in WT P60 = 1.8 ± 0.2, $p = 0.02$; Table 1). Moreover, ClC-5 expression

←

only in the length and amino acid composition of the N terminus. * (asterisk) indicates fully conserved residues. ***A*** : (colon) denotes conserved residues with strong similar properties and a . (period) indicates conserved residues of weakly similar properties. ***B***, Confocal images of chromaffin cells expressing ClC-3c-eGFP/mRFP (ClC-3c promoter-driven expression) together with markers for large dense-core vesicles. ClC-3c-eGFP/mRFP with mRFP-VAMP3 *(a)*, NPY-mRFP *(b)*, Chromogranin ChrA-eGFP *(c)*, mRFP-VAMP4 *(d)*. ***C***, Confocal pictures showing the colocalization of ClC-3c-eGFP in recycling endosomes, positive for mRFP-Rab11 *(a)* and transferrin receptor TfR-mRFP *(b)*. ***D***, Mander¨s coefficient analyses for all colocalization experiments. More than 70% of ClC-3c positive puncta colocalize with VAMP3, Rab11, or with TfR and >50% with NPY, ChrA, or with VAMP4 but not with Lamp1, indicating that a large fraction of ClC-3c protein resides mainly in a subpopulation of LDCV positive for recycling endosomes (VAMP3). In contrast, ClC-3b shows extensive colocalization with LAMP1 but negligible colocalization with VAMP3 or with Rab11. Data were collected from four independent cultures, ClC-3c/VAMP3, $n = 11$; ClC-3c/NPY, $n = 12$; ClC-3c/ChrA, $n = 11$; ClC-3c/VAMP4, $n = 10$; ClC-3c/Rab11, $n = 10$; ClC-3c/TfR; $n = 10$; ClC-3c/Lamp1, $n = 10$; ClC-3b/VAMP3, $n = 16$; ClC-3/Rab11, $n = 10$; ClC-3b/Lamp1, $n = 12$. All data are represented as mean ± SEM. ***E***, Representative confocal images from chromaffin cells coexpressing the splice variant ClC-3b-eGFP together with mRFP-VAMP3 *(a)* or with the recycling endosomal markers mRFP-Rab11 *(b)*, or the lysosomal marker Lamp1-mRFP *(c)*. Note that ClC-3b accumulates in the membrane of large vesicle structures that exhibit a high degree of colocalization with the lysosomal marker Lamp1 *(c)* but not with VAMP3 *(a)* nor with the recycling endosomal marker Rab11 *(b)*. ClC-3c-eGFP describes different subcellular distribution than Lamp1-mRFP *(d)*. Inset, Areas outlined in white boxes. Line scan analyses (bottom, each confocal image) for the corresponding protein illustrating that subcellular distribution pattern at both channels (dashed lines). Scale bars: 5 μm; insets, 1 μm. *n* denotes the numbers of cells analyzed.

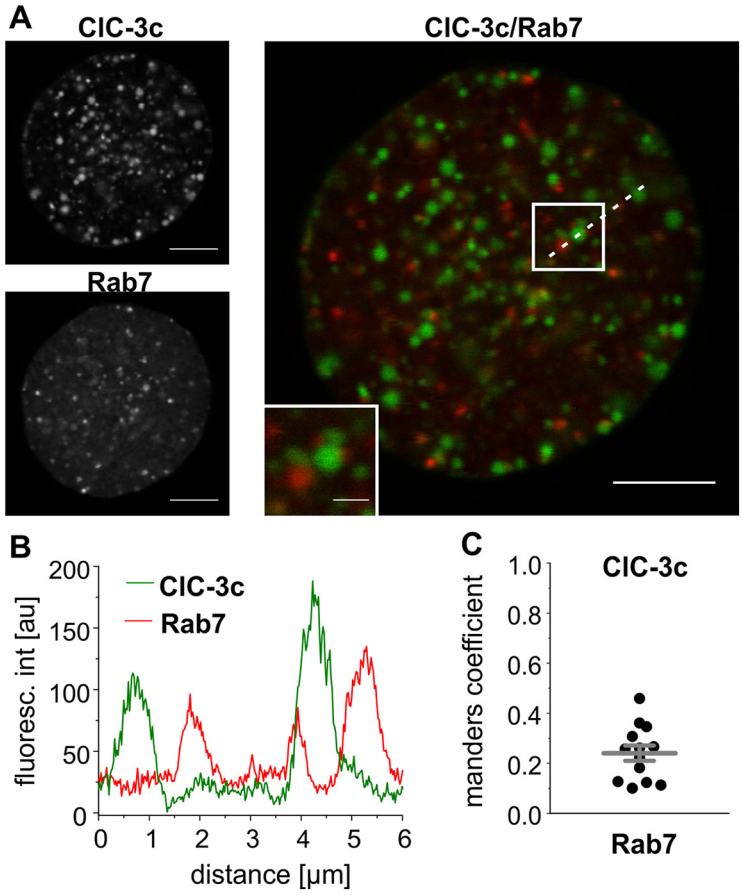

Figure 6. ClC-3c does not localize to late endosomes. ***A***, Representative confocal image of chromaffin cells coexpressing ClC-3c-eGFP together with the late endosomal marker mRFP-Rab7. Inset, Areas outlined in white boxes; dashed line within the image represents a linear section of the image analyzed in (***B***). Scale bars: 5 µm; insets, 1 µm. ***B***, Line scan analysis, dashed line in (***A***) illustrating that ClC-3c exhibits a different subcellular distribution than Rab7. ***C***, Mander's coefficient analysis for ClC-3c/Rab7 colocalization experiments. ClC-3c positive puncta do not colocalize with Rab7. ClC-3c/Rab7, $n = 13$. Data are collected from three independent transfected cultures and represented as mean ± SEM; *n* denotes the number of analyzed cells.

is upregulated in *Clcn3*$^{-/-}$ adrenal glands, (Log [cDNA] = 2.7 ± 0.2 for ClC-5 in WT P0 vs in 3.1 ± 0.15 for ClC-5 in *Clcn3*$^{-/-}$ P0, $p = 0.02$; Table 1). Altogether, these data show an age-dependent reduction in the ClC-5 mRNA expression levels that are associated with changes in the density of voltage-gated calcium channels.

ClC-3c localizes to a subpopulation of LDCVs that is positive for VAMP3/cellubrevin

There are five splice variants of *Clcn3*—ClC-3a, ClC-3b, ClC-3c, ClC-3d, and ClC-3e—that reside in distinct intracellular compartments (Gentzsch et al., 2003; Okada et al., 2014; Guzman et al., 2015). We tested the expression of ClC-3 in mouse adrenal glands using RT-PCR and found not only all *Clcn3* splice variants but also ClC-5 in this tissue (Fig. 3*A*). In cultured mammalian cells, ClC-3a and ClC-3b localize to the lysosome (Guzman et al., 2015) and ClC-3e to the Golgi apparatus (Gentzsch et al., 2003). The exact subcellular localization of ClC-3d is currently not known; however, carboxy-terminal sequences are identical in ClC-3d and ClC-3e, suggesting that ClC-3d also localizes to Golgi (Okada et al., 2014; Fig. 4*A*). ClC-3c is sorted to the recycling endosome (RE) of HEK293T cells (Guzman et al., 2015) and thus represents a candidate Cl^-/H^+ exchanger in chromaffin cell LDCVs.

As there are no ClC-3-specific antibodies available that permit distinction between endosomal ClC-3 splice variants (Fig. 5), we expressed ClC-3b and ClC-3c as eGFP-fusion proteins in chromaffin cells and studied their subcellular localization using confocal microscopy and Mander's correlation coefficient (Fig. 4*B–E*). To avoid overexpression artifact, we used the mouse ClC-3c promoter to drive the expression of ClC-3. Cells transduced with the exogenous ClC-3b or ClC-3c reached nearly the same mRNA transcripts levels as in the WT condition (endogenous ClC-3c 6.3e-3 ± 0.4e-3 vs exogenous ClC-3c 7.0e-3 ± 0.3e-3 $p = 0.1$ and endogenous ClC-3b 2.1e-2 ± 0.4e-2 vs exogenous ClC-3b 2.2e-2 ± 1.0e-2 $p = 0.1$; $n = 4$-5 cultures, Mann–Whitney rank sum test). Chromaffin cells were cotransfected with fluorescently tagged markers, such as VAMP3/cellubrevin, VAMP4, Chromogranin A (ChrA), or neuropeptide Y (NPY), amd were coexpressed together with ClC-3c or ClC-3b. VAMP3 is a vSNARE protein present in recycling endosomes (Teter et al., 1998) and implicated in the exocytosis of chromaffin granules (Borisovska et al., 2005), NPY and ChrA are markers for LDCVs (Huttner et al., 1995), and VAMP4 has been used to identify immature LDCVs (Eaton et al., 2000; Bonnemaison et al., 2013). We found ClC-3c, but not ClC-3b, preferentially in a subpopulation of LDCV that are positive for VAMP3 (Fig. 4*B(a),E(a),D*). ClC-3b localizes to lysosomes (Fig. 4*E(c),D*), in agreement with Maritzen et al. (2008), but not to the recycling endosome (Fig. 4*E(b),D*). In contrast, >70% of ClC-3c positive puncta colocalize with VAMP3 and >50% with NPY or ChrA and with VAMP4 (Fig. 4*B(b–d),D*). There are two functionally distinct populations of recycling endosomes that either express Rab11 (Kobayashi and Fukuda, 2013) or the transferrin receptor TfR (Maxfield and McGraw, 2004). In agreement with our previous work (Guzman et al., 2015), we found colocalization of ClC-3c with both recycling endosomal marker Rab11 and TfR (Ullrich et al., 1996; Kobayashi and Fukuda, 2013; Fig. 4*C(a,b),D*), whereas colocalization with the lysosomal/late endosomal marker Lamp1/Rab7 was negligible (Figs. 4*E(d),D*, 6). These results identify ClC-3c as the ClC-3 splice variant present at a subpopulation of VAMP3-positive LDCVs.

Expression of ClC-3c but not of ClC-3b fully rescues exocytosis in double mutant *Clcn3*$^{-/-}$/*kd*ClC-5 cells

Photolytic uncaging of Ca^{2+} causes a homogeneous step-like increase in the intracellular calcium concentration ($[Ca^{2+}]_i$) from ~300 nM to ~30 µM that synchronizes fusion of catecholamine-containing vesicles and permits quantifying the time course of vesicle fusion (Fig. 7*A*). In such experiments, three kinetically distinct release components can be separated by fitting the capacitance time course with the sum of two exponentials and a linear function; the exocytotic burst, in which the RRP and the SRP of vesicles fuse with the membrane (Voets et al., 1999), and the sustained component, which reflects the continuous priming and fusion of granules at high $[Ca^{2+}]_i$ (Rettig and

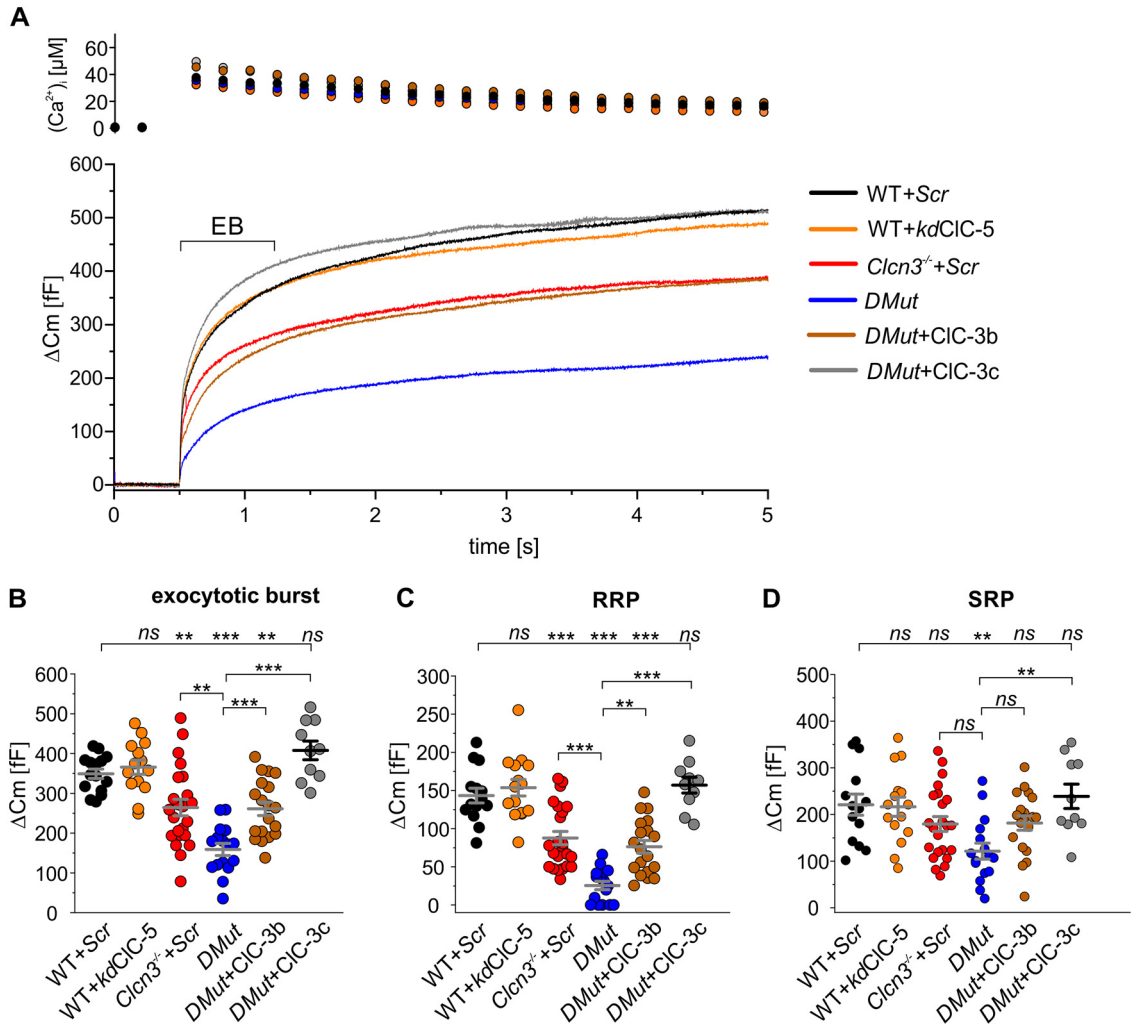

Figure 7. Cl^-/H^+ exchangers regulate exocytosis of LDCVs in chromaffin cells. ***A***, Averaged $[Ca^{2+}]_i$ (top) and corresponding capacitance responses to flash stimulation from WT chromaffin cells expressing scrambled shRNA (WT+*Scr*, black trace) or shRNA against *Clcn5* (knock down, WT+*kd*ClC-5, orange trace) or from $Clcn3^{-/-}$ cells expressing scrambled shRNA ($Clcn3^{-/-}$+*Scr*, red trace) or shRNA against *Clcn5* (*DMut*; $Clcn3^{-/-}$+*kd*ClC-5, blue trace) or the different rescue conditions; ClC-3b or ClC-3c (*DMut*+ClC-3b, brown trace, and *DMut*+ClC-3c, gray trace). ***B***, Changes of the exocytotic burst in response to flash stimulation from virally transduced WT or $Clcn3^{-/-}$ chromaffin cells expressing different constructs (WT+*Scr*, $n = 14$, black circles, WT+*kd*ClC-5, $n = 14$, orange circles; $Clcn3^{-/-}$+*Scr*, $n = 23$, red circles; *DMut*, $n = 16$, blue circles; *DMut*+ClC-3b, $n = 19$, brown circles; *DMut*+ClC-3c, $n = 10$, gray circles). ***C***, ***D***, Knock down of ClC-5 in $Clcn3^{-/-}$ cells (*DMut*, blue circles) selectively reduce the size of the fast component of vesicle exocytosis (RRP; ***C***), leaving the slow component (SRP) almost unaffected (***D***). Rescue experiments illustrate the ability of Cl^-/H^+ exchangers in restoring exocytosis of LDCVs in *Dmut* conditions. WT+*Scr*, $n = 14$, black circles; WT+*kd*ClC-5, $n = 14$, orange circles; $Clcn3^{-/-}$+*Scr*, $n = 23$, red circles; *DMut*, $n = 16$, blue circles; *DMut*+ClC-3b, $n = 19$; *DMut*+ClC-3c, $n = 10$, gray circles. $^{***}p < 0.001$, $^{**}p < 0.01$. ns, Not significant. Groups of data were statistically analyzed by comparing them to WT+*Scr* or *DMut* using one-way ANOVA (Tukey's HSD *post hoc* test). Data were collected from four to five independent cultures per condition and are represented as mean ± SEM. n denotes the number of analyzed cells.

Neher, 2002). When calcium channels are bypassed with flash photolysis, the absence of ClC-3 indeed attenuates the exocytotic response in young cells (Fig. 7). The exocytotic burst as well as its two components of release, the RRP and SRP, are reduced in $Clcn3^{-/-}$+*Scr* cells (Fig. 7*B–D*), without changes in time constants, and the sustained component of release remains unaltered. The reduced changes in membrane cell capacitance during exocytotic bursts might be because of smaller vesicles in the $Clcn3^{-/-}$ condition. We quantified the size of LDCV by electron microscopy and did not find differences in size distributions of LDCV between $Clcn3^{-/-}$ and WT condition from P0–P1 mice (Fig. 8*A*,*B*). On average, we obtained LDCVs diameters of 141.3 ± 2.6 nm in WT and 147.7 ± 5.0 nm in $Clcn3^{-/-}$ ($p = 0.3$, Mann–Whitney rank sum test, Fig. 8*C*), similar to values reported for mice at this age (Pinheiro et al., 2014). We conclude that the absence of ClC-3 does not alter the size of the LDCVs in chromaffin cells but rather the availability of vesicles for exocytosis.

We next corrected for the upregulation of ClC-5 in $Clcn3^{-/-}$ by using lentivirus-mediated shRNA transfer [$Clcn3^{-/-}$/*kd*ClC-5, hereafter denoted as double mutant (*DMut*) cells]. As controls, WT or $Clcn3^{-/-}$ cells were transduced with a virus carrying the scrambled shRNA sequence (hereafter denoted as +*Scr*). *DMut* cells showed a significant reduction of the ClC-5 mRNA expression levels 4–5 d after lentiviral transduction (mRNA ClC-5 levels relative to 18S for WT+*Scr* = 0.014 ± 1.5e-3 and for *kdClC-5* = 9.62e-4 ± 1.99e-5, $p < 0.003$, $n = 8$ cultures, Student©s *t* test). Deletion of ClC-5 in $Clcn3^{-/-}$ cells leads to a further reduction of the exocytotic burst in the flash-evoked vesicle exocytosis by ~40% ($Clcn3^{-/-}$+*Scr* 264.2 ± 20.8 fF vs *DMut* 158.9 ± 15.3 fF, $p < 0.001$) so that responses of *DMut* chromaffin cells were 54% smaller than in WT+*Scr* cells (WT+*Scr* 349.1 ± 11.9 fF vs *DMut* 158.9 ± 15.3 fF, $p < 0.001$; Fig. 7*A*,*B*).

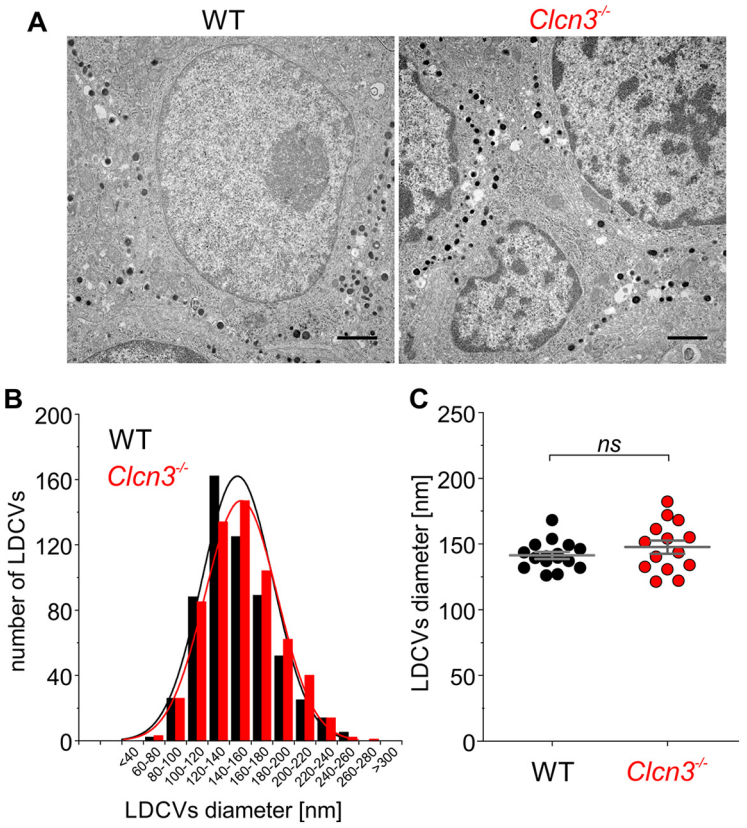

Figure 8. Ablation of ClC-3 does not alter the size of LDCVs in chromaffin cells. ***A***, Electron micrographs of a representative field of view from WT and *Clcn3*$^{-/-}$ condition. ***B***, Histogram of the diameter distribution of LDCVs in electron micrograph from WT and *Clcn3*$^{-/-}$ (black, WT, 580 vesicles; red, *Clcn3*$^{-/-}$, 618 vesicles). ***C***, Mean LDCV diameter (black, WT, 16 different fields of view; red, *Clcn3*$^{-/-}$, 14 different fields of view, $p = 0.3$). Data were collected from two independent animal preparations and are represented as mean ± SEM. ns, Not significant. Student's *t* test. Scale bar: 1 μm.

Reduced ClC-5 expression in *Clcn3*$^{-/-}$ cells mainly impaired the size of the fast phase (RRP), whereas the slow phase (SRP) of the exocytotic burst remained almost unaffected (Fig. 7*C*,*D*). The subsequent sustained component of the release, as well as the release time constant of the RRPs, was not altered by the absence of both transporters (*DMut*). Knock down of ClC-5 in WT cells did not change the exocytotic response (Fig. 7, orange trace and circles), arguing against an independent upstream function of ClC-5 in granule exocytosis.

Expression of ClC-3c in *DMut* cells completely restores the flash-evoked response (Fig. 7*B*–*D*). The exocytotic burst and its two components of release were significantly different from the *DMut*, but similar to control (Fig. 7*B*–*D*). ClC-3b expression was less effective in rescuing the exocytotic response (Fig. 7*A*). The magnitude of the exocytotic burst was similar in *DMut*+*ClC-3b* cells to that observed in *Clcn3*$^{-/-}$+*Scr* cells (Fig. 7*B*). The size of the RRP was almost identical to the *Clcn3*$^{-/-}$+*Scr* condition but significantly higher than that of the *DMut* cells, and the SRP was not statistically different from the *DMut* (Fig. 7*C*,*D*). Expression of the exogenous ClC-3c or 3b in *DMut* cells resulted in similar mRNA transcript levels of the splice variants as in the WT condition (endogenous ClC-3c 6.3e-3 ± 0.4e-3 vs exogenous ClC-3c 7.0e-3 ± 0.3e-3 $p = 0.1$ and endogenous ClC-3b 2.1e-2 ± 0.4e-2 vs exogenous ClC-3b 2.2e-2 ± 1.0e-2 $p = 0.1$; $n = 4$–5 cultures, Mann–Whitney rank sum test). We can therefore exclude the possibility that the rescue phenotypes are a consequence of lentiviral ClC-3c or ClC-3b overexpression. The rescue experiments indicate that ClC-3c is sufficient to support granule exocytosis and can fully substitute for the loss of Cl^-/H^+ exchangers in secretory vesicles. They suggest that ClC-3c is present in LDCVs, which is in good agreement with our confocal results.

ClC-3c but not ClC-3b contributes to catecholamine accumulation in secretory granules

The absence of ClC-3 Cl^-/H^+ exchangers is predicted to alter the luminal ionic composition of chromaffin granules and thus their neurotransmitter content. To assess the catecholamine content of individual secretory vesicles and define the contribution of ClC-3c and ClC-3b to catecholamine accumulation, we used carbon fiber amperometry and stimulated secretion by extracellular application of 80 mM of potassium solution or by infusion of 3 μM of free Ca^{2+}. On stimulation with high K^+, which mimics electrical stimulation with >15Hz (Fulop and Smith, 2007), spike amplitudes and charges (which reports on the vesicular catecholamine content) as well as frequencies of the amperometric signal were significantly smaller in *DMut* than in WT+*Scr* (Fig. 9*A*–*E*); half-width and 50–90% rise times were unchanged (Fig. 9*F*,*G*). No differences in any amperometric parameter were observed between *Clcn3*$^{-/-}$+*Scr* and *DMut* (Fig. 9*B*–*G*). Expression of ClC-3c in *DMut* cells restored WT event frequency, amplitude, and charge (Fig. 9*B*–*D*). In contrast, expression of ClC-3b in *DMut* left quantal sizes as small as in *DMut* cells (Fig. 9*B*–*D*), with no changes in the half-width and in the rise time (Fig. 9*F*,*G*). Event frequency in *DMut*+ClC-3b cells was not significantly different from the *DMut* or WT+*Scr*; however, frequencies values were below those obtained in WT+*Scr* or *DMut*+ClC-3c conditions (Fig. 9*E*). The foot signal (Table 2) was comparable for WT and in absence of both transporters and not changed on expression of ClC-3b or ClC-3c, indicating that Cl^-/H^+ exchangers are not involved in the fusion pore formation of secretory granules.

Infusion of 3 μM free Ca^{2+} permits resolving individual secretory responses independently of voltage-gated calcium channel opening. However, Ca^{2+} infusion does not only trigger the fusion of highly primed vesicles but also the unprimed pool of vesicles. In *DMut*, amperometry experiments confirmed the reduced catecholamine content of secretory granules in the absence of both transporters (Fig. 10, *DMut*). The amplitude, frequency, and quantal charge were significantly reduced in *DMut* cells when compared with the WT+*Scr* condition (Fig. 10*A*–*E*). The half-width of *DMut* fusion events triggered by intracellular Ca^{2+} infusion was larger than that of WT+*Scr*-mediated events (Fig. 10*B*,*F*) but unaltered on stimulation by K^+ perfusion. Expression of ClC-3c rescued the frequency and the quantal size in *DMut* cells also for this stimulation paradigm to WT levels (Fig. 10*C*–*E*). The rescue was only evident during the first 40 s of amperometric recording, suggesting that only newly formed vesicles were equipped with the transduced protein (Duncan et al., 2003; Estévez-Herrera et al., 2016; Fig. 11). Again, expression of ClC-3b in *Dmut* cells (*DMut*+ClC-3b) failed to restore the

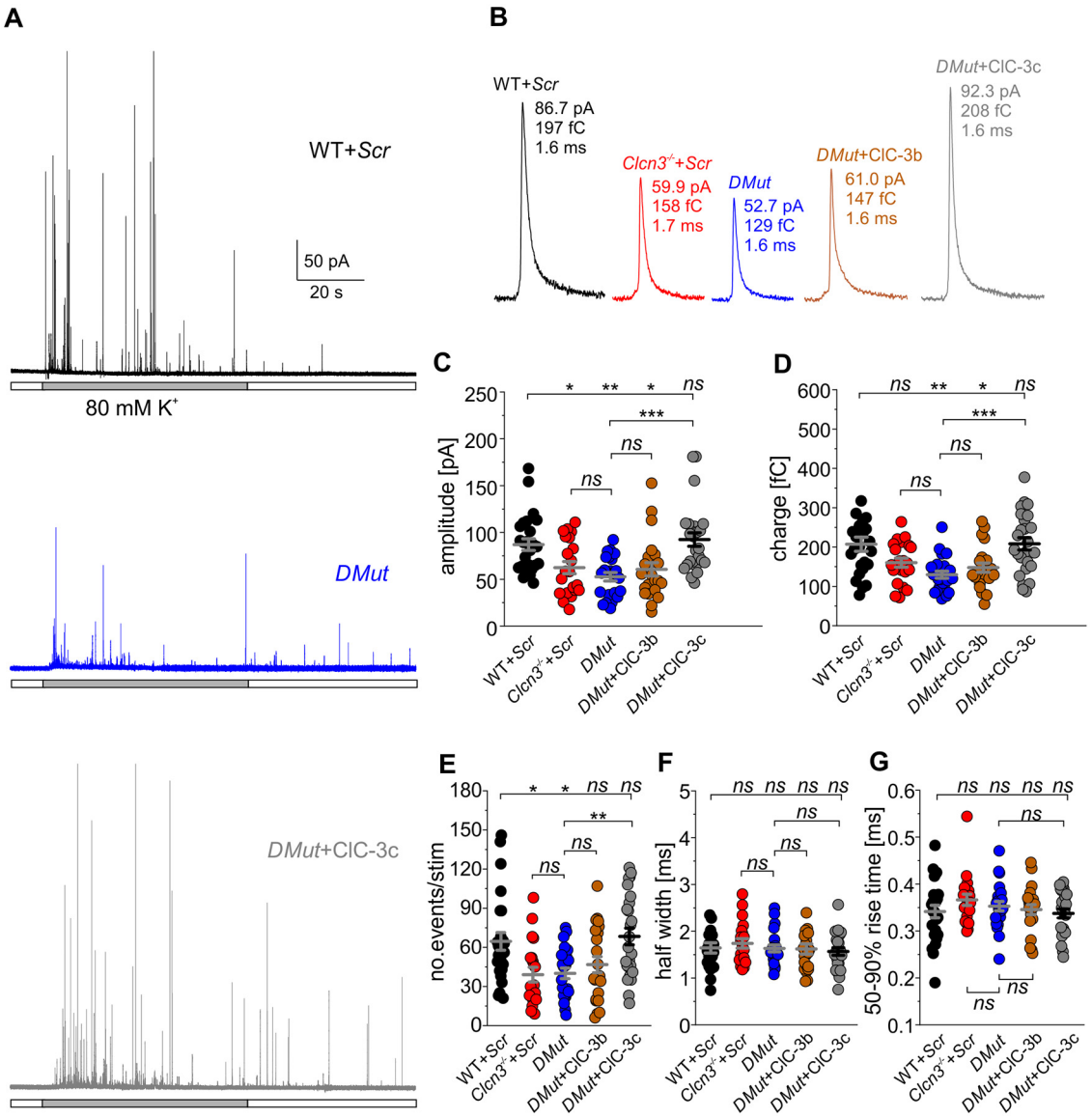

Figure 9. ClC-3c but not ClC-3b regulates catecholamine accumulation in chromaffin granules. ***A***, Representative amperometric traces for WT+*Scr*, *DMut*, or *DMut*+ClC-3c condition. Secretion of catecholamine was triggered by the application of a high K^+-extracellular solution (80 mM KCl, 60 s duration). ***B***, Representative single exocytotic events from amperometric recordings on WT+*Scr* (black), *Clcn3*$^{-/-}$+*Scr*, (red), *DMut* (blue), *DMut*+ClC-3b (brown), or *DMut*+ClC-3c (gray). ***C–G***, Properties of secretory amperometric events for WT+*Scr* ($n = 24$, black circles), *Clcn3*$^{-/-}$+*Scr*, ($n = 20$, red circles), *DMut* ($n = 23$, blue circles), *DMut*+ClC-3b ($n = 21$, brown circles), or *DMut*+ClC-3c ($n = 25$, gray circles), represented as data distribution. ***$p < 0.001$, **$p < 0.01$, *$p < 0.05$. ns, Not significant. The different conditions were compared with WT+*Scr* or *DMut* using one-way ANOVA (Tukey's HSD *post hoc* test). Data were collected from seven independent experiments per condition and are represented as mean ± SEM. n denotes the number of analyzed cells.

Table 2. Properties of individual fusion events stimulated by extracellular application of high [K^+] solution in WT or *Clcn3*$^{-/-}$ chromaffin cells expressing scrambled/eGFP (WT+*scr* or *Clcn3*$^{-/-}$+*scr*) or *Clcn3*$^{-/-}$ chromaffin cells expressing *kd*ClC-5 (*DMut*) or *kd*ClC-5+ClC-3b (*DMut*+ClC-3b) or *kd*ClC-5+ClC-3c (*DMut*+ClC-3c)

						Foot parameters			
Genotype (no. of cells)	No. events/ stimulus	Charge (pC)	Amplitude (pA)	50–90% Rise time (ms)	Half-width (ms)	% of events with foot	Foot amplitude (pA)	Foot duration (ms)	Foot charge (fC)
WT+*Scr* ($n = 24$)	64.6 ± 7.0	0.206 ± 0.02	86.9 ± 6.2	0.34 ± 0.01	1.6 ± 0.1	41 ± 2.5	5.3 ± 0.2	8.1 ± 0.6	46.0 ± 4.2
Clcn3$^{-/-}$+*Scr* ($n = 20$)	39.0 ± 5.6*	0.158 ± 0.01*	59.9 ± 6.3*	0.37 ± 0.01^{ns}	1.7 ± 0.1^{ns}	43.7 ± 3.4^{ns}	4.7 ± 0.3^{ns}	8.6 ± 0.8^{ns}	44.5 ± 4.7^{ns}
DMut ($n = 23$)	40.0 ± 4.0*	0.129 ± 0.009***	52.7 ± 4.5**	0.35 ± 0.01^{ns}	1.6 ± 0.1^{ns}	43 ± 3.4^{ns}	4.7 ± 0.3^{ns}	7.4 ± 0.5^{ns}	36.7 ± 3.8^{ns}
DMut+*ClC-3b* ($n = 21$)	46.7 ± 6.1$^{ns/\mathbf{ns}}$	0.147 ± 0.011*/$^{\mathbf{ns}}$	61.0 ± 7.4*/$^{\mathbf{ns}}$	0.34 ± 0.01$^{ns/\mathbf{ns}}$	1.6 ± 0.1$^{ns/\mathbf{ns}}$	43.5 ± 3.9$^{ns/\mathbf{ns}}$	4.8 ± 0.4$^{ns/\mathbf{ns}}$	7.8 ± 0.6$^{ns/\mathbf{ns}}$	38.8 ± 4.6$^{ns/\mathbf{ns}}$
DMut+*ClC-3c* ($n = 25$)	68.3 ± 6.4$^{ns/\dagger\dagger}$	0.208 ± 0.016$^{ns/\dagger\dagger\dagger}$	92.3 ± 7.2$^{ns/\dagger\dagger\dagger}$	0.34 ± 0.01$^{ns/\mathbf{ns}}$	1.6 ± 0.1$^{ns/\mathbf{ns}}$	47.7 ± 2.5$^{ns/\mathbf{ns}}$	5.3 ± 0.3$^{ns/\mathbf{ns}}$	9.2 ± 0.5$^{ns/\mathbf{ns}}$	46.6 ± 3.8$^{ns/\mathbf{ns}}$

No. of events/stimulus refers to the mean number of amperometric events obtained during the application of 80 mM potassium solution (60 s application). ***$p < 0.001$, **$p < 0.01$, *$p < 0.05$, ns; Not significant, versus WT+*scr* and $^{\dagger\dagger\dagger}p < 0.001$, $^{\dagger\dagger}p < 0.01$, $^{\dagger}p < 0.05$, *ns*, Not significant, versus *DMut*. One-way ANOVA (Tukey's HSD *post hoc* test). Data were collected from five to seven independent experiments per condition and are represented as mean ± SEM. Bold-italic ns represent the statistical comparison of the different rescues versus the *DMut*.

Table 3. Properties of individual fusion events stimulated by intracellular perfusion of 3 μM free Ca^{2+} solution in WT chromaffin cells expressing scrambled/eGFP (WT+*scr*) or *Clcn3*$^{-/-}$ chromaffin cells expressing *kd*ClC-5 (*DMut*) or *kd*ClC-5+ClC-3b (*DMut*+ClC-3b) or *kd*ClC-5+ClC-3c (*DMut*+ClC-3c)

Genotype (no. of cells/total no. of events)	Event frequency (Hz)	Charge (pC)	Amplitude (pA)	50–90% Rise time (ms)	Half-width (ms)	Foot parameters: % of events with foot	Foot amplitude (pA)	Foot duration (ms)	Foot charge (fC)
WT+*Scr* (n = 23/1462)	1.6 ± 0.24	0.241 ± 0.01	97.7 ± 5.0	0.33 ± 0.01	1.6 ± 0.1	25.9 ± 1.8	6.0 ± 0.4	6.3 ± 0.5	42.1 ± 4.4
DMut (n = 20/801)	0.84 ± 0.11*	0.163 ± 0.009***	52.2 ± 4.2***	0.35 ± 0.01 ^{ns}	1.9 ± 0.1*	23.8 ± 2.2 ^{ns}	4.7 ± 0.3 ^{ns}	5.5 ± 0.3 ^{ns}	28.0 ± 2.5*
DMut+*ClC-3b* (n = 18/717)	0.8 ± 0.1$^{*/ns}$	0.139 ± 0.01$^{***/ns}$	64.8 ± 7.7$^{**/ns}$	0.32 ± 0.01 $^{ns/ns}$	1.4 ± 0.1 $^{ns/†††}$	23.9 ± 2.3 $^{ns/ns}$	4.7 ± 0.5 $^{ns/ns}$	5.6 ± 0.4 $^{ns/ns}$	31.6 ± 4.5 $^{ns/ns}$
DMut+*ClC-3c* (n = 17/1375)	1.9 ± 0.19 $^{ns/†††}$	0.224 ± 0.015 $^{ns/†}$	95.8 ± 6.1 $^{ns/†††}$	0.32 ± 0.01 $^{ns/†}$	1.5 ± 0.1 $^{ns/††}$	29.5 ± 3.0 $^{ns/ns}$	5.6 ± 0.2 $^{ns/ns}$	4.8 ± 0.3 $^{ns/ns}$	30.0 ± 1.9 $^{ns/ns}$

No. of cells/total no. of events denotes the number of cell and the total number of events analyzed per condition. Event frequency was calculated over the first 40 s of amperometric recording. ***$p < 0.001$, **$p < 0.01$, *$p < 0.05$; ns, Not significant, versus WT+*scr* and $^{†††}p < 0.001$, $^{††}p < 0.01$, $^{†}p < 0.05$, *ns*, Not significant, versus *DMut*. One-way ANOVA (Tukey's HSD *post hoc* test). data were collected from four to five independent experiments per condition and are represented as mean ± SEM. Bold-italic ns represent the statistical comparison of the different rescues versus the *DMut*.

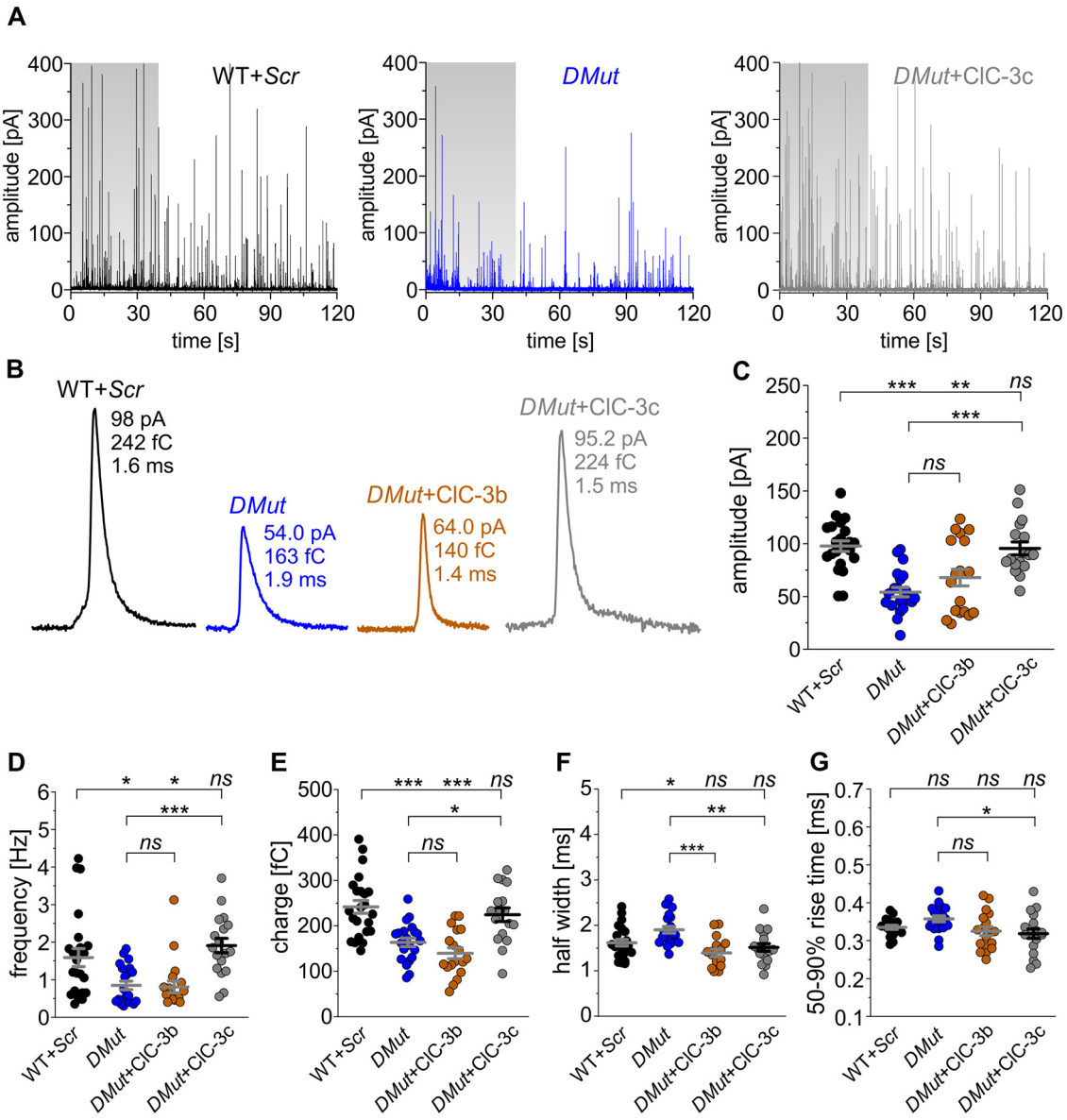

Figure 10. Ca^{2+} infusion experiments confirm the Cl^{-}/H^{+} exchanger dependency of the catecholamine accumulation process. ***A***, Representative amperometric recording for WT, *DMut*, or *DMut*+ClC-3c (area highlighted in gray within the recording represents the first 40 s of analyses showed in ***C–G***) stimulated by the pipette infusion of 3 μM free Ca^{2+}. ***B***, Representative single exocytotic events from amperometric recordings on WT+*Scr* (black), *DMut* (blue), *DMut*+ClC-3b (brown), or *DMut*+ClC-3c (gray). Spikes with values closer to the mean average amplitude, charge, and half for each condition were selected within the amperometric recordings. ***C–G***, Properties of secretory amperometric events for WT+*Scr* (n = 23 cells, black circles, with 63.5 ± 9.6 events per cells), *DMut* (n = 20 cells, blue circles; with 33.9 ± 4.5 events per cell), *DMut*+ClC-3b (n = 18 cells, brown circles; with 31.2 ± 5.46 events per cells), or *DMut*+ClC-3c (n = 17 cells, gray circles; with 76.4 ± 7.7 events per cells), represented as data distribution. ***$p < 0.001$, **$p < 0.01$, *$p < 0.05$. ns, Not significant. Different conditions were compared with the WT+*Scr* or *DMut* using one-way ANOVA (Tukey's HSD *post hoc* test). Data were collected from four independent experiments per condition and are represented as mean ± SEM.

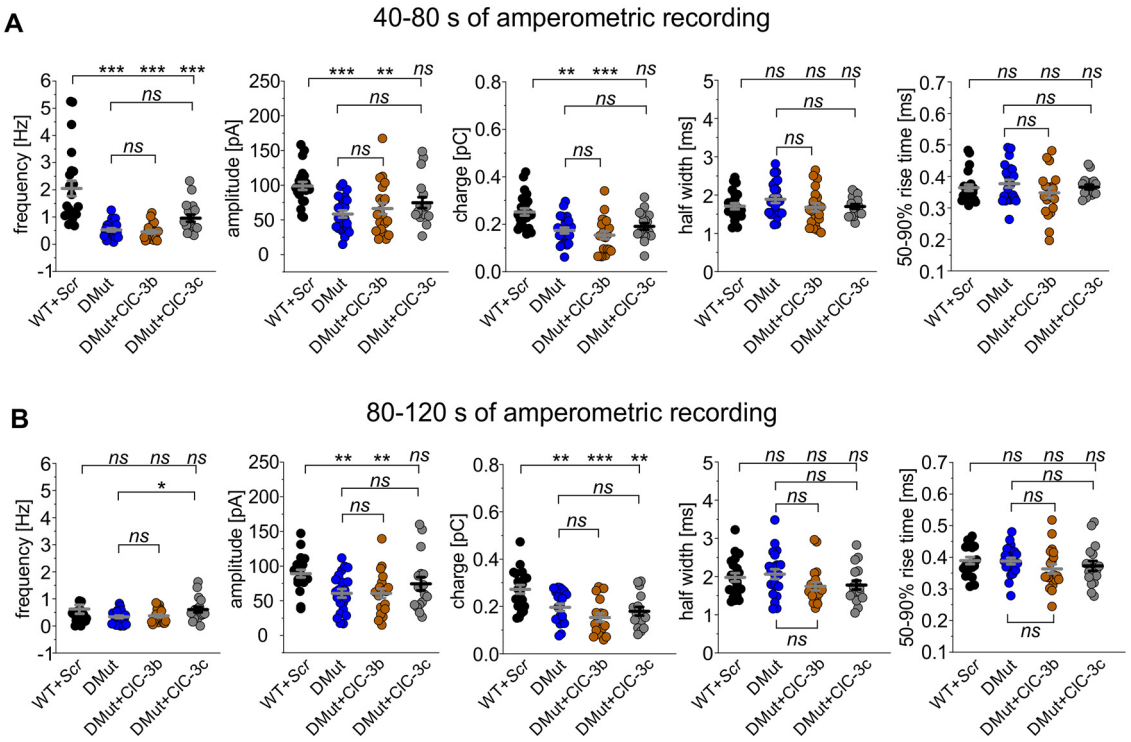

Figure 11. Analyses of single amperometric events. ***A–B***, Properties of secretory amperometric events for WT+*Scr* ($n = 23$, black circles), *DMut* ($n = 20$, blue circles), *DMut*+ClC-3b ($n = 18$, brown circles), or *DMut*+ClC-3c ($n = 17$, gray circles). Represented data distribution within 40–80 s in (***A***) and 80–120 s and in (***B***) of amperometric recording. Data information: $^{***}p < 0.001$, $^{**}p < 0.01$, $^{*}p < 0.05$. ns, Not significant, Data were compared with WT+*Scr* using one-way ANOVA (Tukey's HSD *post hoc* test). Data were collected from four to five independent experiments per condition and are represented as mean ± SEM; *n* denotes the number of analyzed cells.

catecholamine content of the individual secretory granules; quantal amplitude and charge were significantly smaller than in the WT+*Scr* but not statistically different from *DMut* (Fig. 10*C*, *E*). Event frequency was not different between *DMut*+ClC-3b and *DMut*. ClC-3b and ClC-3c did not cause major changes in foot signal or in the 50–90% rise time of the amperometry currents (Fig. 10*G*, Table 3), reinforcing the notion that Cl^-/H^+ exchangers are not involved in the formation and expansion of the fusion pore of secretory granules. Expression of ClC-3b or ClC-3c both accelerated the half-width to values closer to WT+*Scr* condition (Fig. 10*F*). The presence of ClC-3c but not of ClC-3b in secretory vesicles is in line with the notion that Cl^-/H^+ exchangers are required to regulate the vesicular catecholamine content of chromaffin granules.

Discussion

We here studied the role of CLC Cl^-/H^+ exchangers in chromaffin cells. We found that one ClC-3 splice variant, ClC-3c, localizes to the LDCVs, regulates the catecholamine accumulation process, and efficiently contributes to the establishment of secretory granules for exocytosis. ClC-3b is not present in LDCVs and does not regulate the granular neurotransmitter content. It contributes to vesicle priming, but only with reduced efficiency. ClC-5 is developmentally downregulated in WT chromaffin cells, and ClC-3 deficiency causes compensatory changes in the ClC-5 mRNA expression levels.

The contribution of Cl^-/H^+ exchangers to granule exocytosis in chromaffin cells can be demonstrated in rescue experiments, in which exocytosis was triggered by flash photolysis of caged calcium (Fig. 7). The expression of ClC-3c in double Cl^-/H^+ exchanger-deficient cells fully rescues the exocytotic response of secretory granules to WT levels (Fig. 7, *DMut*+ClC-3c), showing that ClC-3c is essential and functionally sufficient for neurosecretion. In contrast, the expression of ClC-3b in *DMut* cells supports exocytosis with low efficiency (Fig. 7, *DMut*+ClC-3b). In the absence of ClC-3, upregulation of ClC-5 (Table 1) was not able to compensate for the flash-evoked response (Fig. 7, *Clcn3*$^{-/-}$+*Scr*). Its removal in WT cells does not alter granule exocytosis (Fig. 7, WT+*kd*ClC-5), indicating that ClC-5 plays a minor, if any, role in exocytosis in WT condition.

To study the fusion of individual vesicles we used two different experimental approaches, high K^+ or Ca^{2+}-infusion stimulation (Figs. 9, 10). We used amperometry to analyze the quantal neurotransmitter content of the chromaffin granules and found reduced quantal amperometric charges in the absence of ClC-3 alone (Fig. 9, *Clcn3*$^{-/-}$) or absence of ClC-3 and ClC-5 (*DMut*; Figs. 9, 10). Because the size of LDCVs is similar in WT and *Clcn3*$^{-/-}$ (Fig. 8), such reduction must be caused by differences in LDCV catecholamine concentrations. In rescue experiments from *DMut* cells, the expression of ClC-3c was the only Cl^-/H^+ exchanger that fully recovers all amperometric parameters to control levels (Figs. 9, 10). Lentiviral expression of ClC-3b left quantal sizes in *DMut* cells unaffected (Figs. 9, 10), indicating that only ClC-3c, but not ClC-3b, contributes to catecholamine accumulation. None of our genetic maneuvers changed the prespike signal or the rise time of amperometric events (Figs. 9*G*, 10*G*, Tables 2, 3), arguing against an important role of ClC-3 in the initial formation and expansion of the fusion pores in chromaffin granules. Application of 80 mM of extracellular K^+ as well as Ca^{2+} infusion lead to a fast increase in the cytosolic Ca^{2+} at the release site and promotes full-collapse vesicle exocytosis (Elhamdani et al., 2001; Fulop and Smith, 2007). The observed smaller unitary events in *DMut* under such full-collapse fusion

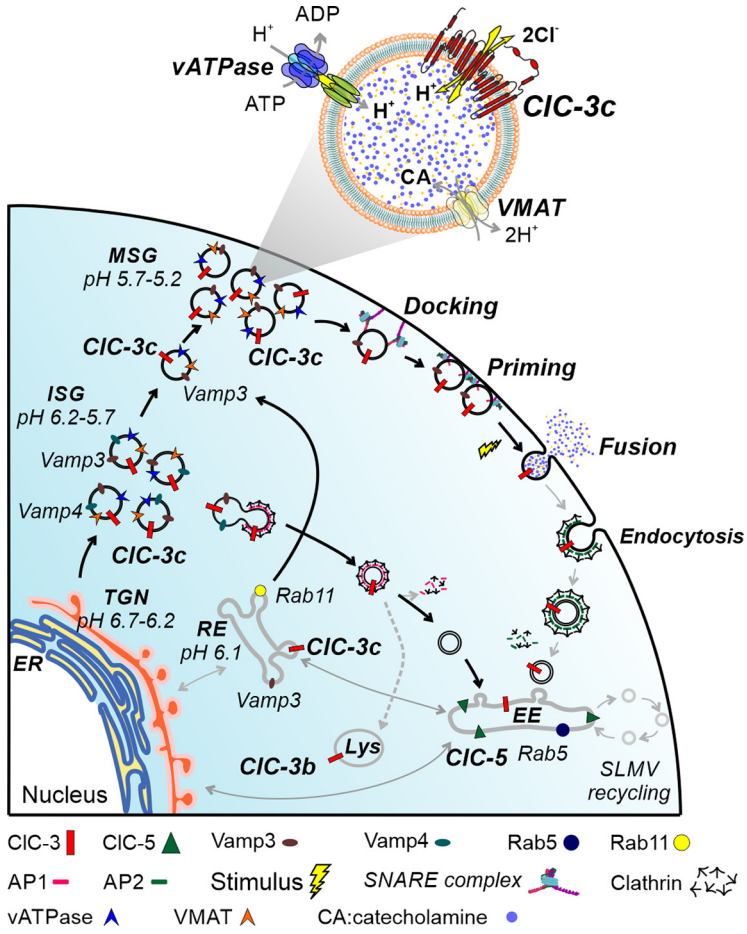

Figure 12. Proposed functions and subcellular localization of CLC-type Cl^-/H^+ exchangers in neurosecretion.

exclude the possibility of partial catecholamine discharge from mutant granules.

This functional evidence is in good agreement with our colocalization analyses. It supports the notion that ClC-3c, but not ClC-3b, is present in LDCVs, with ClC-3c in a subpopulation of LDCV positive for VAMP3 and ClC-3b in lysosomes (Fig. 4). Our conclusion that ClC-3c is present in LDCVs disagrees with earlier reports on the ClC-3 localization in chromaffin cells. Maritzen et al. (2008) used immunolabeling and viral infection to conclude that ClC-3 neither colocalizes with chromogranin in chromaffin cells, a marker for secretory granules, nor with insulin in β-pancreatic cells. The discrepancy between these and our results is likely because of the existence of multiple splice variants with distinct subcellular localization. The antibodies used in the earlier study cannot differentiate between splice variants, and Maritzen et al. (2008) virally expressed only ClC-3b, so no conclusion can be drawn about ClC-3c from these experiments. Weinert et al. (2020) used localization experiments with fluorescently tagged ClC-3 and functional studies to conclude that ClC-3 is not present in synaptic vesicles. They took advantage of a novel knock-in mouse model (*Clcn3*$^{ven/ven}$) with a Venus tag sequence fused to the start of exon 1. This genetic modification results in the expression of only certain fluorescently tagged *Clcn3* splice variants, that is, of ClC-3a (M_007711.3), but not of others, most importantly not of ClC-3c. Moreover, Weinert et al. (2020) assessed synaptic transmission in hippocampal slices and found that the frequency and amplitude of quantal events were similar between WT and *Clcn3*$^{-/-}$; however, the authors did not correct for the upregulation of ClC-5 at the age in which the experiments were performed (P14–16). The novel experiments of Weinert et al. (2020) thus do not contradict the functional role of ClC-3c in exocytosis.

CLC antiporters might affect the recycling of other proteins that regulate catecholamine secretion. Genetic ablation of SNAP-25, a SNARE protein essential for Ca^{2+}-dependent exocytosis in neuroendocrine cells, causes defective priming of LDCVs (Sørensen et al., 2003, Washbourne et al., 2002) and alters Ca^{2+} current densities in chromaffin cells (Toft-Bertelsen et al., 2016), quite similar to the *Clcn3*$^{-/-}$ phenotype. However, deletion of SNAP-25 leaves the neurotransmitter content of individual granules unaffected (Sørensen et al., 2003), thus excluding the possibility that a trafficking defect of SNAP-25 is the sole basis of the observed functional alterations. Secretory vesicles contain a granule matrix that binds catecholamines (Helle et al., 1985). Two major constituents, chromogranin A and B, have been identified and shown to be involved in granulogenesis as well as in catecholamine sequestration (Videen et al., 1992; Yoo, 1996; Kim et al., 2006; Díaz-Vera et al., 2012). The absence of chromogranin A/B in chromaffin cells reduces the quantal charge and the frequency of amperometric events (Díaz-Vera et al., 2012), similar to the *DMut* phenotype. However, whereas deletion of chromogranin A/B affects the rising phase of quantal events, the *DMut*-mediated events do not show changes in the kinetic of fusion neither by high K^+ stimulation nor by Ca^{2+}infusion; the rise time was affected by the double ClC deletion (Figs. 9, 10). This indicates that a reduced granular content of granins is not responsible for the *DMut* phenotype.

Figure 12 depicts our current concepts about the functions of ClC-3b and ClC-3c in chromaffin cells. After exocytosis, chromaffin granule components are retrieved through the early endosome to the trans-Golgi network (Ceridono et al., 2011), and nascent granules undergo additional maturation steps that involve reduction of the luminal pH (Kim et al., 2006). VMATs exchange one catecholamine for two luminal protons so that pH gradients across the LDCV membrane are main determinants of the vesicular catecholamine content. ClC-3 is a chloride/proton exchanger, and its pronounced voltage dependence makes ClC-3 perfectly suited for chloride-driven vesicle acidification (Guzman et al., 2013; Rohrbough et al., 2018). Our results are compatible with the idea that ClC-3c regulates the catecholamine accumulation process by fine-tuning the luminal ion concentration of secretory vesicles. ClC-3c traffics from the trans-Golgi network to REs and consequently to immature secretory granule, where it might contribute to reducing the luminal pH as a maturation step. Lack of ClC-3 impairs vesicle acidification and makes catecholamine accumulation less efficient, resulting in lower levels of neurotransmitters. ClC-3b contributes to vesicle priming (Fig. 7*C*, *DMut*+ClC-3b) and is unable to restore the quantal content (Figs. 9, 10, *DMut*+ClC-3b), suggesting that ClC-3b is present at an early stage of vesicle maturation and is subsequently sorted to

the lysosomes (Fig. 12). In addition to modifying the vesicular ion homeostasis, ClC-3 might also recruit novel binding partners that modify secretory vesicle pools (Weinert et al., 2014).

We observed increased densities of voltage-gated calcium channels (Fig. 2) and ClC-5 mRNA transcript levels in chromaffin cells from young *Clcn3*$^{-/-}$ mice (Table 1). Moreover, exocytosis elicited by a train of depolarizing pulses was significantly impaired in adults but not in young *Clcn3*$^{-/-}$ cells (Fig. 1). These results suggest that ClC-5 regulates the trafficking of calcium channels in an early developmental stage. *Clcn5* is the disease gene for Dent's disease (Fisher et al., 1995), and its gene product, ClC-5, was shown to be involved in endocytosis of various epithelial cells (Piwon et al., 2000). Age-dependent downregulation in neuronal tissues, as well as the lack of neurologic symptoms in Dent's disease patients (Wrong et al., 1994), suggested that ClC-5 does not play an important role in the mature CNS. Our work on chromaffin cells—a model system for presynaptic function—demonstrates how regulating the expression of ClC-5 minimizes the impact of ClC-3 ablation on exocytosis by increasing the number of calcium channels on the plasma membrane. This mechanism predicts a neuroprotective function of ClC-5 in neuronal cells, which likely prevents neurodegeneration in *Clcn3*$^{-/-}$ before P20 (Stobrawa et al., 2001).

Our results identify ClC-3 as a key element of the regulated exocytotic pathway of neuroendocrine cells. They indicate that ClC-3c plays an active role in the neurotransmitter accumulation process, most likely adjusting luminal ionic concentrations of secretory vesicles and thereby facilitating catecholamine uptake. This work pinpoints the subcellular role of ClC-3 in neuroexocytosis and sets down the bases for a better understanding of the functions of Cl^-/H^+ exchangers in cellular physiology.

References

Barg S, Huang P, Eliasson L, Nelson DJ, Obermüller S, Rorsman P, Thévenod F, Renström E (2001) Priming of insulin granules for exocytosis by granular Cl^- uptake and acidification. J Cell Sci 114:2145–2154.

Becherer U, Rettig J (2006) Vesicle pools, docking, priming, and release. Cell Tissue Res 326:393–407.

Bonnemaison ML, Eipper BA, Mains RE (2013) Role of adaptor proteins in secretory granule biogenesis and maturation. Front Endocrinol (Lausanne) 4:101.

Borisovska M, Zhao Y, Tsytsyura Y, Glyvuk N, Takamori S, Matti U, Rettig J, Südhof T, Bruns D (2005) v-SNAREs control exocytosis of vesicles from priming to fusion. EMBO J 24:2114–2126.

Burack MA, Silverman MA, Banker G (2000) The role of selective transport in neuronal protein sorting. Neuron 26:465–472.

Ceridono M, Ory S, Momboisse F, Chasserot-Golaz S, Houy S, Calco V, Haeberlé AM, Demais V, Bailly Y, Bader MF, Gasman S (2011) Selective recapture of secretory granule components after full collapse exocytosis in neuroendocrine chromaffin cells. Traffic 12:72–88.

Choudhury A, Dominguez M, Puri V, Sharma DK, Narita K, Wheatley CL, Marks DL, Pagano RE (2002) Rab proteins mediate Golgi transport of caveola-internalized glycosphingolipids and correct lipid trafficking in Niemann-Pick C cells. J Clin Invest 109:1541–1550.

Deriy LV, Gomez EA, Jacobson DA, Wang X, Hopson JA, Liu XY, Zhang G, Bindokas VP, Philipson LH, Nelson DJ (2009) The granular chloride channel ClC-3 is permissive for insulin secretion. Cell Metab 10:316–323.

Dhara M, Yarzagaray A, Schwarz Y, Dutta S, Grabner C, Moghadam PK, Bost A, Schirra C, Rettig J, Reim K, Brose N, Mohrmann R, Bruns D (2014) Complexin synchronizes primed vesicle exocytosis and regulates fusion pore dynamics. J Cell Biol 204:1123–1140.

Díaz-Vera J, Camacho M, Machado JD, Domínguez N, Montesinos MS, Hernández-Fernaud JR, Luján R, Borges R (2012) Chromogranins A and B are key proteins in amine accumulation, but the catecholamine secretory pathway is conserved without them. FASEB J 26:430–438.

Duncan RR, Greaves J, Wiegand UK, Matskevich I, Bodammer G, Apps DK, Shipston MJ, Chow RH (2003) Functional and spatial segregation of secretory vesicle pools according to vesicle age. Nature 422:176–180.

Eaton BA, Haugwitz M, Lau D, Moore HP (2000) Biogenesis of regulated exocytotic carriers in neuroendocrine cells. J Neurosci 20:7334–7344.

Elhamdani A, Palfrey HC, Artalejo CR (2001) Quantal size is dependent on stimulation frequency and calcium entry in calf chromaffin cells. Neuron 31:819–830.

Estévez-Herrera J, Domínguez N, Pardo MR, Gonález-Santana A, Westhead EW, Borges R, Machado JD (2016) ATP: the crucial component of secretory vesicles. Proc Natl Acad Sci U S A 113:E4098–E4106.

Fisher SE, van Bakel I, Lloyd SE, Pearce SH, Thakker RV, Craig IW (1995) Cloning and characterization of CLCN5, the human kidney chloride channel gene implicated in Dent disease (an X-linked hereditary nephrolithiasis). Genomics 29:598–606.

Fulop T, Smith C (2007) Matching native electrical stimulation by graded chemical stimulation in isolated mouse adrenal chromaffin cells. J Neurosci Methods 166:195–202.

Galli T, Zahraoui A, Vaidyanathan VV, Raposo G, Tian JM, Karin M, Niemann H, Louvard D (1998) A novel tetanus neurotoxin-insensitive vesicle-associated membrane protein in SNARE complexes of the apical plasma membrane of epithelial cells. Mol Biol Cell 9:1437–1448.

Gentzsch M, Cui L, Mengos A, Chang XB, Chen JH, Riordan JR (2003) The PDZ-binding chloride channel ClC-3B localizes to the Golgi and associates with cystic fibrosis transmembrane conductance regulator-interacting PDZ proteins. J Biol Chem 278:6440–6449.

Guzmán RE, Bolaños P, Delgado A, Rojas H, DiPolo R, Caputo C, Jaffe EH (2007) Depolymerisation and rearrangement of actin filaments during exocytosis in rat peritoneal mast cells: involvement of ryanodine-sensitive calcium stores. Pflugers Arch 454:131–141.

Guzman RE, Schwarz YN, Rettig J, Bruns D (2010) SNARE force synchronizes synaptic vesicle fusion and controls the kinetics of quantal synaptic transmission. J Neurosci 30:10272–10281.

Guzman RE, Grieschat M, Fahlke C, Alekov AK (2013) ClC-3 is an intracellular chloride/proton exchanger with large voltage-dependent nonlinear capacitance. Acs Chem Neurosci 4:994–1003.

Guzman RE, Miranda-Laferte E, Franzen A, Fahlke C (2015) Neuronal ClC-3 splice variants differ in subcellular localizations, but mediate identical transport functions. J Biol Chem 290:25851–25862.

Guzman RE, Bungert-Plümke S, Franzen A, Fahlke C (2017) Preferential association with ClC-3 permits sorting of ClC-4 into endosomal compartments. J Biol Chem 292:19055–19065.

Helle KB, Reed RK, Pihl KE, Serck-Hanssen G (1985) Osmotic properties of the chromogranins and relation to osmotic pressure in catecholamine storage granules. Acta Physiol Scand 123:21–33.

Huttner WB, Ohashi M, Kehlenbach RH, Barr FA, Bauerfeind R, Bräunling O, Corbeil D, Hannah M, Pasolli HA, Schmidt A (1995) Biogenesis of neurosecretory vesicles. Cold Spring Harb Symp Quant Biol 60:315–327.

Jentsch TJ, Maritzen T, Keating DJ, Zdebik AA, Thevenod F (2010) ClC-3–a granular anion transporter involved in insulin secretion? Cell Metab 12:307–308.

Kim T, Gondre-Lewis MC, Arnaoutova I, Loh YP (2006) Dense-core secretory granule biogenesis. Physiology (Bethesda) 21:124–133.

Kobayashi H, Fukuda M (2013) Arf6, Rab11 and transferrin receptor define distinct populations of recycling endosomes. Commun Integr Biol 6: e25036.

Li DQ, Jing X, Salehi A, Collins SC, Hoppa MB, Rosengren AH, Zhang E, Lundquist I, Olofsson CS, Mörgelin M, Eliasson L, Rorsman P, Renström E (2009) Suppression of sulfonylurea- and glucose-induced insulin secretion in vitro and in vivo in mice lacking the chloride transport protein ClC-3. Cell Metab 10:309–315.

Maritzen T, Keating DJ, Neagoe I, Zdebik AA, Jentsch TJ (2008) Role of the vesicular chloride transporter ClC-3 in neuroendocrine tissue. J Neurosci 28:10587–10598.

Maxfield FR, McGraw TE (2004) Endocytic recycling. Nat Rev Mol Cell Biol 5:121–132.

Mishima T, Fujiwara T, Sanada M, Kofuji T, Kanai-Azuma M, Akagawa K (2014) Syntaxin 1B, but not syntaxin 1A, is necessary for the regulation of synaptic vesicle exocytosis and of the readily releasable pool at central synapses. PLoS One 9:e90004.

Okada T, Akita T, Sato-Numata K, Islam MR, Okada Y (2014) A newly cloned ClC-3 isoform, ClC-3d, as well as ClC-3a mediates Cd-sensitive outwardly rectifying anion currents. Cell Physiol Biochem 33:539–556.

O'Leary NA, Wright MW, Brister JR, Ciufo S, Haddad D, McVeigh R, Rajput B, Robbertse B, Smith-White B, Ako-Adjei D, Astashyn A, Badretdin A, Bao Y, Blinkova O, Brover V, Chetvernin V, Choi J, Cox E, Ermolaeva O, Farrell CM, et al. (2016) Reference sequence (RefSeq) database at NCBI: current status, taxonomic expansion, and functional annotation. Nucleic Acids Res 44:D733–D745.

Pinheiro PS, Jansen AM, De Wit H, Tawfik B, Madsen KL, Verhage M, Gether U, Sorensen JB (2014) The BAR domain protein PICK1 controls vesicle number and size in adrenal chromaffin cells. J Neurosci 34:10688–106700.

Piwon N, Günther W, Schwake M, Bösl MR, Jentsch TJ (2000) ClC-5 Cl--channel disruption impairs endocytosis in a mouse model for Dent's disease. Nature 408:369–373.

Rettig J, Neher E (2002) Emerging roles of presynaptic proteins in Ca^{++}-triggered exocytosis. Science 298:781–778.

Rohrbough J, Nguyen HN, Lamb FS (2018) Modulation of ClC-3 gating and proton/anion exchange by internal and external protons and the anion selectivity filter. J Physiol 596:4091–4119.

Schneider CA, Rasband WS, Eliceiri KW (2012) NIH Image to ImageJ: 25 years of image analysis. Nat Methods 9:671–675.

Schoch S, Deák F, Königstorfer A, Mozhayeva M, Sara Y, Südhof TC, Kavalali ET (2001) SNARE function analyzed in synaptobrevin/VAMP knockout mice. Science 294:1117–1122.

Sherer NM, Lehmann MJ, Jimenez-Soto LF, Ingmundson A, Horner SM, Cicchetti G, Allen PG, Pypaert M, Cunningham JM, Mothes W (2003) Visualization of retroviral replication in living cells reveals budding into multivesicular bodies. Traffic 4:785–801.

Sørensen JB, Nagy G, Varoqueaux F, Nehring RB, Brose N, Wilson MC, Neher E (2003) Differential control of the releasable vesicle pools by SNAP-25 splice variants and SNAP-23. Cell 114:75–86.

Stauber T, Jentsch TJ (2010) Sorting motifs of the endosomal/lysosomal CLC chloride transporters. J Biol Chem 285:34537–34548.

Stauber T, Jentsch TJ (2013) Chloride in vesicular trafficking and function. Annu Rev Physiol 75:453–477.

Stobrawa SM, Breiderhoff T, Takamori S, Engel D, Schweizer M, Zdebik AA, Bösl MR, Ruether K, Jahn H, Draguhn A, Jahn R, Jentsch TJ (2001) Disruption of ClC-3, a chloride channel expressed on synaptic vesicles, leads to a loss of the hippocampus. Neuron 29:185–196.

Teter K, Chandy G, Quiñones B, Pereyra K, Machen T, Moore HP (1998) Cellubrevin-targeted fluorescence uncovers heterogeneity in the recycling endosomes. J Biol Chem 273:19625–19633.

Toft-Bertelsen TL, Ziomkiewicz I, Houy S, Pinheiro PS, Sørensen JB (2016) Regulation of Ca^{2+} channels by SNAP-25 via recruitment of syntaxin-1 from plasma membrane clusters. Mol Biol Cell 27:3329–3341.

Ullrich O, Reinsch S, Urbé S, Zerial M, Parton RG (1996) Rab11 regulates recycling through the pericentriolar recycling endosome. J Cell Biol 135:913–924.

Videen JS, Mezger MS, Chang YM, O'Connor DT (1992) Calcium and catecholamine interactions with adrenal chromogranins. Comparison of driving forces in binding and aggregation. J Biol Chem 267:3066–3073.

Voets T, Neher E, Moser T (1999) Mechanisms underlying phasic and sustained secretion in chromaffin cells from mouse adrenal slices. Neuron 23:607–615.

Washbourne P, Thompson PM, Carta M, Costa ET, Mathews JR, Lopez-Benditó G, Molnar Z, Becher MW, Valenzuela CF, Partridge LD, Wilson MC (2002) Genetic ablation of the t-SNARE SNAP-25 distinguishes mechanisms of neuroexocytosis. Nat Neurosci 5:19–26.

Weinert S, Jabs S, Hohensee S, Chan WL, Kornak U, Jentsch TJ (2014) Transport activity and presence of ClC-7/Ostm1 complex account for different cellular functions. EMBO Rep 15:784–791.

Weinert S, Gimber N, Deuschel D, Stuhlmann T, Puchkov D, Farsi Z, Ludwig CF, Novarino G, López-Cayuqueo KI, Planells-Cases R, Jentsch TJ (2020) Uncoupling endosomal CLC chloride/proton exchange causes severe neurodegeneration. EMBO J 39:e103358.

Wrong OM, Norden AG, Feest TG (1994) Dent's disease; a familial proximal renal tubular syndrome with low-molecular-weight proteinuria, hypercalciuria, nephrocalcinosis, metabolic bone disease, progressive renal failure and a marked male predominance. QJM 87:473–493.

Yaffe D, Forrest LR, Schuldiner S (2018) The ins and outs of vesicular monoamine transporters. J Gen Physiol 150:671–682.

Yoo SH (1996) pH- and Ca^{2+}-dependent aggregation property of secretory vesicle matrix proteins and the potential role of chromogranins A and B in secretory vesicle biogenesis. J Biol Chem 271:1558–1565.